Severe Convective Weather Outbreaks on 10 and 15 December 2021: Large-Scale Antecedent Conditions

KIMBERLY A. HOOGEWIND,[a,b] THOMAS J. GALARNEAU JR.,[b] AND VITTORIO A. GENSINI[c]

[a] *Cooperative Institute for Severe and High-Impact Weather Research and Operations, University of Oklahoma, Norman, Oklahoma*
[b] *NOAA/OAR/National Severe Storms Laboratory, Norman, Oklahoma*
[c] *Department of Earth, Atmosphere, and Environment, Northern Illinois University, DeKalb, Illinois*

(Manuscript received 20 October 2024, in final form 22 February 2025, accepted 10 March 2025)

ABSTRACT: The first 2 weeks of December 2021 were exceptionally active for severe convective storms across the central and eastern United States. While previous work has indicated that this was related to the existence of a negative phase of the Pacific–North American pattern, we demonstrate that such a pattern was configured via dynamical linkages between multiple extratropical cyclogenesis events in the western North Pacific, the recurvature of Typhoon Nyatoh, and the subsequent phase evolution of the North Pacific jet. These processes were found to aid in the excitation of Rossby wave packets and the amplification of upper-level flow downstream over the Pacific, ultimately configuring synoptic-scale weather regimes supportive of anomalous high-frequency and high-intensity severe convective weather in the contiguous United States. In addition, abnormally warm Gulf of America/Gulf of Mexico sea surface temperatures, aided by a period of antecedent synoptic-scale subsidence, played a critical role in enhancing convective instability in the surface warm sector. This work underscores the importance of cataloging these events for purposes of examining (and potentially enhancing) predictability.

SIGNIFICANCE STATEMENT: The first half of December 2021 recorded one of the most active cool-season severe weather periods in the United States, resulting in two billion-dollar convective outbreaks on 10 and 15 December. This study links these extreme events to upstream dynamical processes over the North Pacific, including extratropical cyclogenesis, the recurvature of Typhoon Nyatoh, and the retraction of the North Pacific jet. These processes amplified downstream flow and configured synoptic environments favorable for severe weather across the United States. Additionally, anomalously warm Gulf of America/Gulf of Mexico sea surface temperatures enhanced convective instability. By identifying these key precursors, this work highlights the potential for improved anticipation of extended-range severe weather likelihood—particularly during the cool season—when such events remain rare but highly impactful.

KEYWORDS: Cyclogenesis/cyclolysis; Extratropical cyclones; Rossby waves; Severe storms; Synoptic-scale processes; Tropical cyclones

1. Introduction

Climatologically, 1–15 December averages ~17 tornadoes, 27 severe hail reports, and 78 damaging convective wind reports in the United States. In 2021, this same period tallied 215, 85, and 1035 tornado, severe hail, and damage convective gust reports, respectively, helping set a record for the most active December of severe convective weather since records began in the mid-1950s. On 10 December 2021, the deadliest December tornado outbreak on record impacted the mid-Mississippi and Ohio River valleys, resulting in 89 fatalities, 675 injuries, and $4.1 billion in estimated losses. Long-track supercell thunderstorms produced 68 tornado reports, 15 of which were rated EF2, 6 EF3, and 2 EF4 (SPC 2024). Less than a week later, on 15 December, a serial derecho (Johns and Hirt 1987) and tornado outbreak occurred in the central Great Plains and upper Midwest, which resulted in 1 fatality, 2 injuries, and $1.9 billion in estimated damage. In addition to 583 reports of severe winds, including widespread measured gusts of 36–46 m s^{-1}, 125 tornadoes occurred, 33 of which were rated ≥EF2 (SPC 2024).

Boreal cool season (DJF) severe convective weather outbreaks are infrequent but often have a high impact (Childs et al. 2018). Events during this portion of the annual cycle are generally characterized by relatively strong dynamical forcing for ascent, often associated with extratropical cyclones and ample deep-layer wind shear but limited convective instability (e.g., Sherburn and Parker 2014; Sherburn et al. 2016; Wade and Parker 2021). The events on 15 and 10 December 2021 now rank first and second as the most prolific December tornado report days in history, underscoring one of the motivating factors for this work. Due to the significant socioeconomic impact of two multibillion-dollar disasters occurring within 5 days of each other, a question of predictability naturally arises. How far in advance could we have anticipated an active severe weather period? To answer this question, it is important to first diagnose key antecedent physical

Hoogewind's current affiliation: Cooperative Institute for Severe and High-Impact Weather Research and Operations, University of Oklahoma, Norman, Oklahoma and NOAA/NWS/Storm Prediction Center, Norman, Oklahoma.

Corresponding author: Kimberly A. Hoogewind, kimberly.hoogewind@noaa.gov

DOI: 10.1175/MWR-D-24-0213.1

processes that contributed to the amplification of the upper-tropospheric flow evolution in the Northern Hemisphere leading up to the two record-setting outbreaks, and this is the primary objective of the current study. Specifically, this manuscript examines the linkage of multiple extratropical cyclogenesis events in the western North Pacific, recurving Typhoon Nyatoh, the phase of the North Pacific jet (NPJ) stream, and their respective roles in the chronology of the upper-tropospheric flow pattern during the 2-week period preceding the severe weather outbreaks. The organization of this manuscript is as follows. A brief background of work exploring the linkages among recurving tropical cyclones, the NPJ, and extreme weather conditions is presented in section 2. Data and methods are presented in section 3, followed by a synoptic overview of 10 and 15 December 2021 in section 4. Section 4 also documents the dynamical kinematic evolution over the Pacific Ocean and associated contributions from Typhoon Nyatoh and the NPJ. Sections 5 and 6 provide a discussion of findings and conclusions, respectively.

2. Background

Recurving tropical cyclones (TCs) in the western Pacific can have a substantial influence on downstream weather patterns across the contiguous United States (CONUS) (Keller et al. 2019, for a review). When a TC recurves, it may transition from a tropical warm-core system into an extratropical cyclone and interact with the midlatitude westerlies. This process often results in the intensification of the upper-level jetstreak and amplification of the downstream ridge, resulting in the development of Rossby wave packets (RWPs; large-scale thermal troughs and ridges) which transport momentum and heat poleward (e.g., Archambault et al. 2013, 2015; Grams et al. 2015; Keller et al. 2019). In the case of Pacific Ocean TCs, these RWPs can propagate across the Pacific Ocean and into the CONUS, leading to the formation of mid- and upper-level troughs that aid in the dynamical forcing for ascent for extreme weather events and potentially severe convective storms (Cordeira and Bosart 2010; Archambault et al. 2015; Bosart et al. 2017). The precise position and timing of the recurvature of TCs with respect to an approaching trough can significantly alter the downstream atmospheric response (Grams et al. 2013b). For example, Grams et al. (2013b) demonstrated in numerical simulations that downstream response to TC recurvature can be sensitive to the latitude of recurvature, with TCs that were relocated farther north ahead of an approaching trough tending to produce a stronger downstream response, characterized by higher-amplitude Rossby wave trains. The propagation speed of a preexisting upper-level trough can also play a significant role; troughs that do not exhibit eastward acceleration when interacting with a recurving TC are more prone to phase locking and, subsequently, stronger RWP amplification (Riboldi et al. 2019). Ultimately, recurving TCs, particularly those strongly interacting with the NPJ, can significantly alter the position, intensity, and evolution of the NPJ and the downstream upper-tropospheric flow (Archambault et al. 2013, 2015; Winters et al. 2019a).

The influence of the NPJ and recurving TCs on the development of extreme weather across the CONUS during the cool season is also particularly relevant for this work (e.g., Bosart et al. 2017; Winters et al. 2019a; Winters and Attard 2022; Leicht and Bosart 2024). The NPJ has been identified as a key feature in shaping downstream synoptic-scale patterns conducive for temperature and precipitation extremes over the CONUS (Griffin and Martin 2017; Winters et al. 2019a; Winters and Attard 2022). For example, retractions of the NPJ are favorable for cooler and warmer temperatures in the western and eastern United States, respectively (Griffin and Martin 2017; Winters et al. 2019a). This response is primarily related to the fact that NPJ retraction events are commonly followed by the development of a negative Pacific–North American (PNA) pattern (Wallace and Gutzler 1981; Jaffe et al. 2011; Madsen and Martin 2023).

Recurving TCs and NPJ retraction events in the western North Pacific can lead to highly amplified upper-tropospheric flow downstream over North America and have been linked to extreme weather events (e.g., Bosart et al. 2017; Cordeira and Bosart 2010; Leicht and Bosart 2024; Winters et al. 2019a). Yet the antecedent role of recurving TCs interacting with the NPJ to alter CONUS severe convective weather, specifically, remains understudied. This knowledge gap regarding upstream influences motivates this research, particularly in bridging significant spatial and temporal divides between large-scale upstream processes and localized severe convective weather events.

Two recent studies examined atmospheric conditions related to the 10 and 15 December 2021 severe weather outbreaks (Jiang et al. 2023; Kim et al. 2024). In particular, the recurvature of Typhoon Nyatoh in the western North Pacific and its interaction with the NPJ were noted as key contributors to the amplification of the flow pattern over the Pacific and the establishment of a favorable pattern downstream over the CONUS for severe weather (Jiang et al. 2023). As discussed above, this is a very plausible scenario; however, the 5- and 10-daytime mean anomalies used to draw this conclusion cannot account for potentially influential synoptic–dynamic weather processes (e.g., extratropical cyclogenesis events) that occur on shorter time scales. Kim et al. (2024) pointed to a prolonged negative PNA pattern, in place from December 2021 to mid-January 2022, as a key factor in creating favorable conditions for the 10 December tornado outbreak. However, the PNA is a low-frequency mode of intraseasonal variability, and the day-to-day weather patterns over the CONUS may not reflect a composite PNA pattern identified by a daily index. Severe weather outbreaks occur on much shorter time scales ($<$ 1 day), such that linking a persistent ($>$1 month) teleconnection index to a single outbreak day is difficult. Essentially, while these studies offer high-level diagnostic explanations of atmospheric conditions associated with the December 2021 period, they generally focus on longer time scales associated with intraseasonal climate variability. In this study, we provide physical, dynamical underpinning for

explaining structured changes in the NPJ, associated downstream RWP dispersion, and subsequent configuration of the CONUS jet stream pattern on synoptic time scales that favored severe convective weather occurrence.

3. Data and methods

a. Synoptic overview

To provide an overview of December 2021 severe weather events and an analysis of the preceding flow evolution, several different data sources are utilized, including both observational and gridded numerical weather prediction analyses. Severe weather report data and convective outlooks from the Storm Prediction Center (SPC) were aggregated within 24-h periods between 1200 and 1159 UTC to align with the convective day defined by SPC. Surface frontal analyses issued by the Weather Prediction Center (WPC; NOAA 2023) were obtained to provide a summary of relevant weather features. Practically perfect hindcast (PPH) probabilities were computed from severe weather reports following the procedure in Hitchens et al. (2013) and Gensini et al. (2020). The relatively simple procedure involves gridding the observations to an 80-km grid and then applying a Gaussian smoother (σ = 120 km) in the x and y dimensions to arrive at a probability which is approximately equivalent to the spatial scale of SPC probabilistic forecasts of severe weather within 25 mi of a point.

To assess the evolution of the environmental conditions at subdaily temporal frequency, SPC mesoscale surface objective analysis (SFCOA) data were utilized. The SFCOA modifies the surface conditions of the analyses of the Rapid Refresh (RAP) model analyses on a 40-km grid, such that a two-pass Barnes analysis of 2-m temperature and humidity and 10-m winds is utilized as a replacement for the surface fields in the analyses. Additional details about these data can be found in Coniglio and Jewell (2022). The analyses for the operational Global Ensemble Forecast System (GEFS ANL; F000 of the GEFS control member for 0000, 0600, 1200, 1800 UTC initializations) (Guan et al. 2022) were used to analyze the evolution of upstream flow in the Northern Hemisphere, and the GEFS reanalysis serves as the background climatology from which anomalies were computed (Hamill et al. 2022). Last, SST data originate from the geo-polar blended SST analysis, which is an operational high-resolution ≈ 5-km (0.05°) global SST product suite (Maturi et al. 2017).

To characterize the NPJ position, we utilized NPJ phase data from Winters and Attard (2022). The NPJ phase diagram was developed using the first two empirical orthogonal functions (EOFs) of the 250-hPa wind speed over the North Pacific using 21-day moving average during the cool-season months (September–May) (Winters et al. 2019b, their Fig. 4). The zonal and meridional changes in the position of the jet exit region are represented by two principal components (PC), PC1 and PC2, respectively. The resulting NPJ regimes may be classified as retraction, extension, poleward shift, or equatorward shift.

b. Typhoon Nyatoh

The International Best Track Archive for Climate Stewardship (IBTrACS) provided data for the track (central latitude and longitude), intensity information (maximum surface wind speed and minimum mean sea level pressure), and storm classification (e.g., disturbance, depression, tropical storm category, extratropical) for Typhoon Nyatoh (Knapp et al. 2010; Gahtan et al. 2024). The degree of interaction between Typhoon Nyatoh and the jet stream is evaluated using the TC interaction metric of Archambault et al. (2013). The procedure for computing the metric involves first identifying the location and time of occurrence of the maximum interaction, defined as the minimum 250–150-hPa layer averaged potential vorticity (PV) advection by the irrotational wind within a 15° × 30° longitude–latitude search domain poleward of the TC locations for a period 48 h prior to, and 144 h after, the point of recurvature (Riboldi et al. 2019). The Windspharm Python package was used to compute kinematic quantities such as irrotational winds (Dawson 2016). To reduce noise and compare more closely with the results of Archambault et al. (2013) which use coarser 2.5° reanalysis data, the PV on each pressure level is first smoothed with a Gaussian filter (σ = 2.5°) prior to computing advection. Infrared channel brightness temperature from Gridded Satellite (GridSat) data (Knapp et al. 2011) is used to confirm the proximity of the TC cirrus shield, and thus TC outflow, to the maximum interaction point (Archambault et al. 2013). The final quantity of the TC interaction metric is then defined as a 48-h time mean of the PV advection within a 15° × 15° domain centered on the maximum interaction point.

Divergence inversion is used to assess the contribution of TC Nyatoh to the total advection of PV by the irrotational wind along the PV waveguide and upper-level jet. Following a similar methodology as Davis et al. (2008, their section 3), we solve the Poisson equation for velocity potential as

$$\nabla^2 \chi_{\mathrm{TC}} = \begin{cases} \delta : \text{for } r \le 10^\circ \\ 0 : \text{for } r > 10^\circ \end{cases}, \tag{1}$$

where χ_{TC} is the velocity potential within 10° of the TC center, δ is the layer-mean divergence in the 250–150-hPa layer, and r is the radius from the TC center. The irrotational wind attributed to the TC is then computed as

$$V_{\chi_{(\mathrm{TC})}} = \nabla \chi_{\mathrm{TC}}. \tag{2}$$

The background environment irrotational wind with the TC removed is then computed as

$$V_{\chi_{(\mathrm{env})}} = V_{\chi(\mathrm{total})} - V_{\chi(\mathrm{TC})}, \tag{3}$$

where $V_{\chi_{(\mathrm{env})}}$ is the background irrotational wind and $V_{\chi_{(\mathrm{total})}}$ is the total irrotational wind. We compute PV advection by the irrotational wind using $V_{\chi_{(\mathrm{env})}}$ and $V_{\chi_{(\mathrm{total})}}$ and compare the results to evaluate TC Nyatoh's contribution to total PV advection by the irrotational wind.

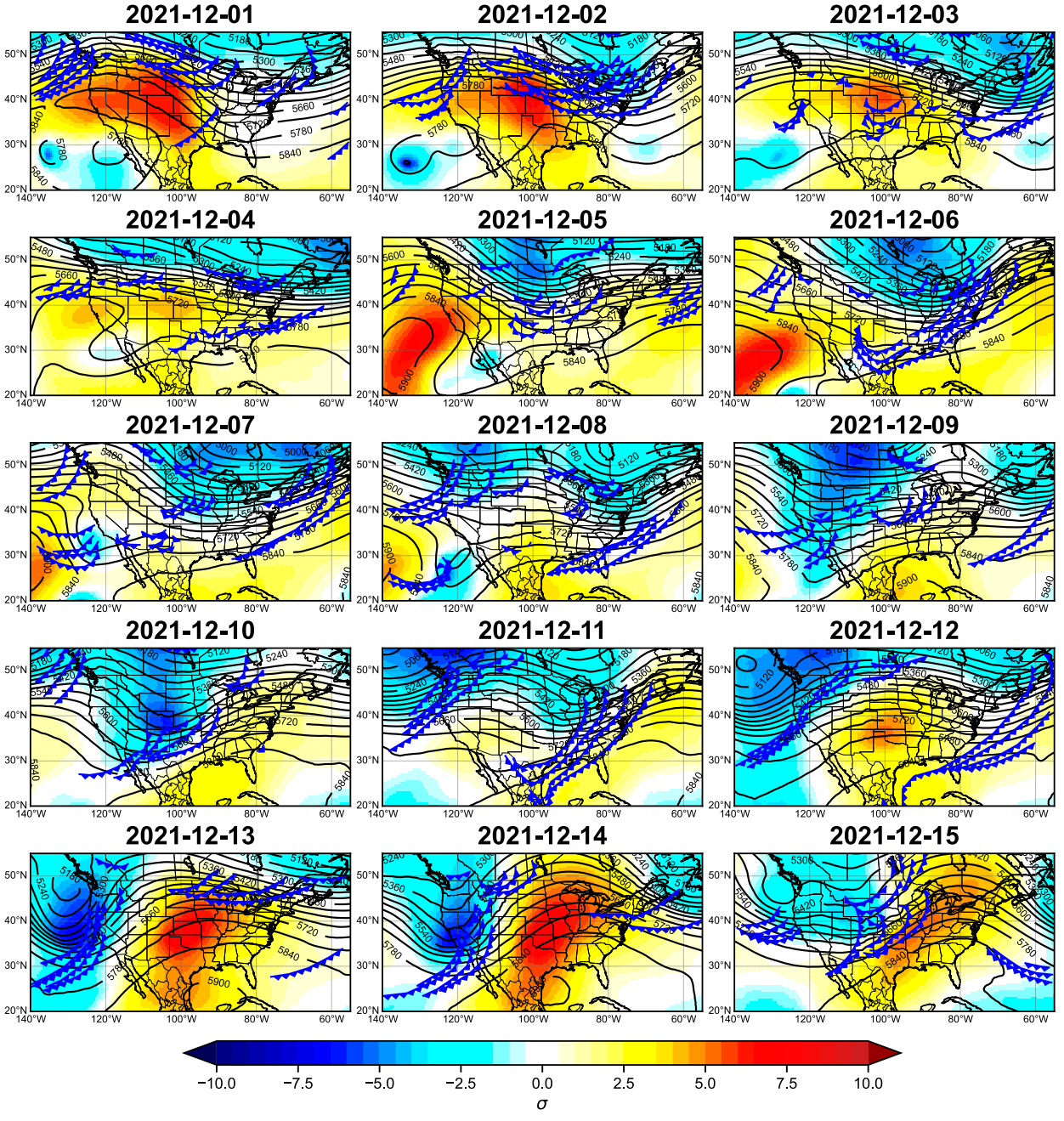

FIG. 1. Daily (1200–1200 UTC) mean GEFS ANL 500-hPa geopotential height (contoured), standardized anomaly (σ; color-filled), and 6-hourly (1200, 1800, 0000, and 0600 UTC) WPC analyzed cold fronts between 1 and 15 Dec 2021.

c. Lagrangian trajectory analyses

To identify air parcel source regions for 1) boundary layer moisture in the severe weather outbreak regions and 2) in the area of a presumed predecessor rain event (PRE) in the area to the northeast of the central location of Typhoon Nyatoh prior to and at the time of maximum interaction with the midlatitude flow, backward trajectory analyses were performed using the Hybrid Single-Particle Lagrangian Integrated Trajectory model (HYSPLIT), developed by the National Oceanic and Atmospheric Administration (NOAA) Air Resources Laboratory (Stein et al. 2015; Rolph et al. 2017). The trajectory analyses used the web-based Real-Time Environmental Applications and Display System (READY) platform and were based upon available archived analyses from the 0.25° Global Forecast System (GFS) analysis data (Rolph et al. 2017). Hourly output of meteorological quantities along each trajectory was used in the analyses.

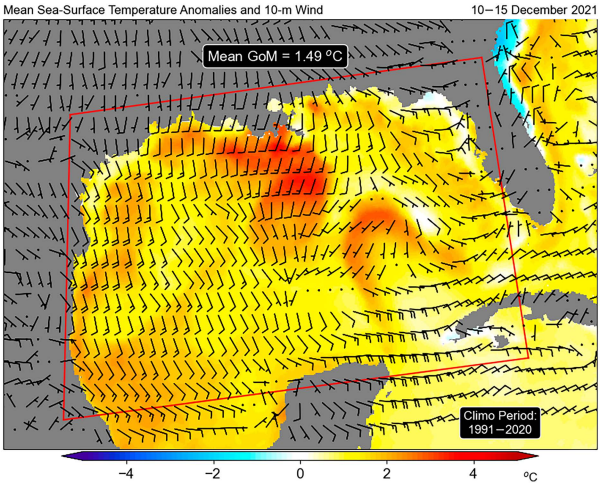

FIG. 2. The GoM mean SST anomalies (°C) and 10-m winds (kt; 1 kt ≈ 0.51 m s^{-1}) during the period 10–15 Dec 2021. Domain-average value bounded by red polygon. SST data described in Maturi et al. (2017).

Following a similar methodology to Molina et al. (2020), backward trajectory analyses are used to identify regions where air parcels acquire moisture leading up to the 10 and 15 December tornado outbreaks. For each event, 72-h backward trajectories are performed for a matrix of points encompassing the primary regions of the respective outbreaks. For 10 December, the trajectories begin at 0000 UTC 11 December and originate at 500 m, roughly the midboundary layer, for a 9 × 11 grid of points with 0.5° latitude–longitude spacing. For 15 December, trajectories are seeded at 2100 UTC for an 11 × 15 matrix of points. Following the method of Sodemann et al. (2008), specific humidity moisture uptake (MU) points are computed along air parcel trajectories to identify near-surface regions where air parcels within the outbreak regions acquired moisture via evaporation. An MU event was defined as a specific humidity increase of ≥2 g kg^{-1} over a 6-h interval at or below the planetary boundary layer (approximated by 900 hPa). The uptake locations and quantities are then mapped to a 160-km grid. The algorithm used to compute MU is based on the PySPLIT package implementation Warner (2018), and for a more detailed description of the process, the reader is referred to Molina et al. (2020) and Sodemann et al. (2008).

4. Results

a. *Synoptic-scale environmental conditions*

1) 1–15 DECEMBER 2021 OVERVIEW

The period from 1 to 15 December 2021 was highly active for severe weather in the central and eastern United States, accounting for 93% of December 2021's total tornadoes. Ten days reported at least one severe weather report, and five of those days (5, 6, 10, 11, and 15 December) were more notable in their

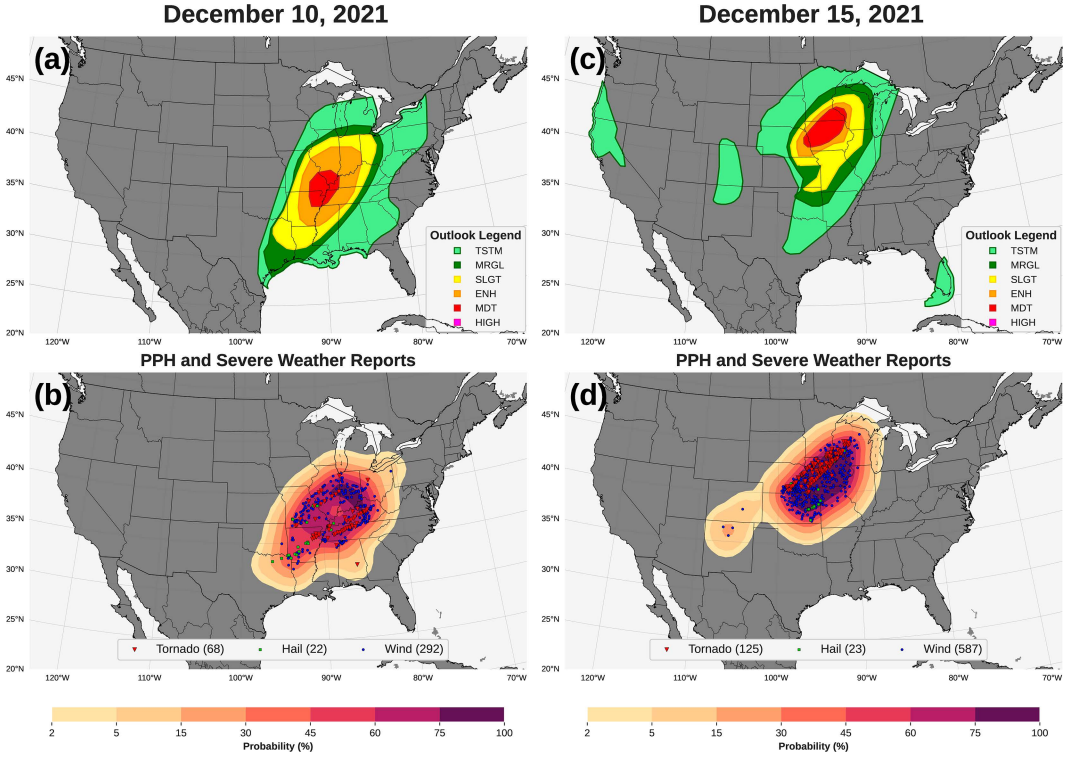

FIG. 3. Daily (1200–1159 UTC) (a),(c) maximum categorical outlook from the SPC (derived from each day 1 categorical outlook product issued) and (b),(d) all severe (tornado, hail, wind) PPH for 10 and 15 Dec 2021.

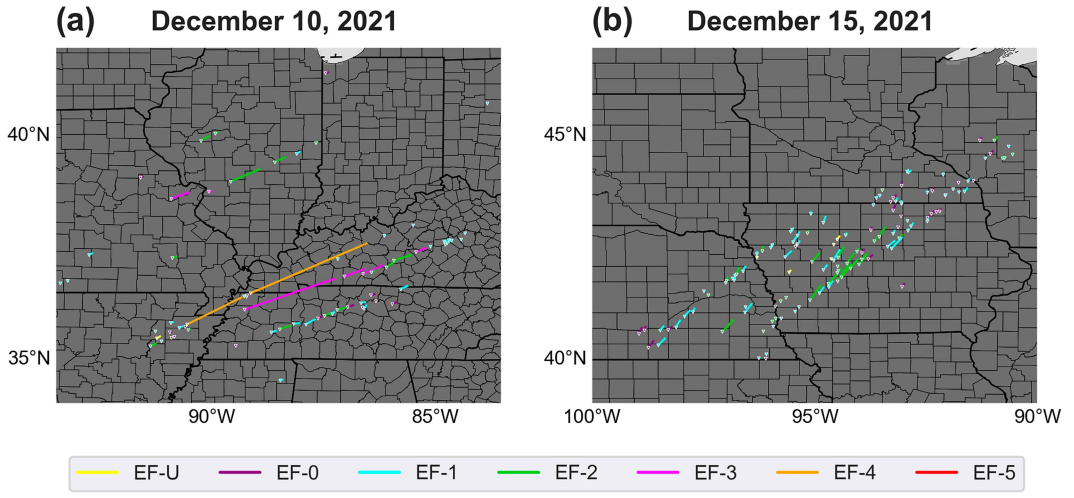

FIG. 4. Tornado tracks for (a) 10 Dec (1200 UTC 10 Dec–1159 UTC 11 Dec) and (b) 15 Dec (1200 UTC 15 Dec–1159 UTC 16 Dec). On 10 Dec, there was one EF0 tornado reported in central Alabama which is not shown.

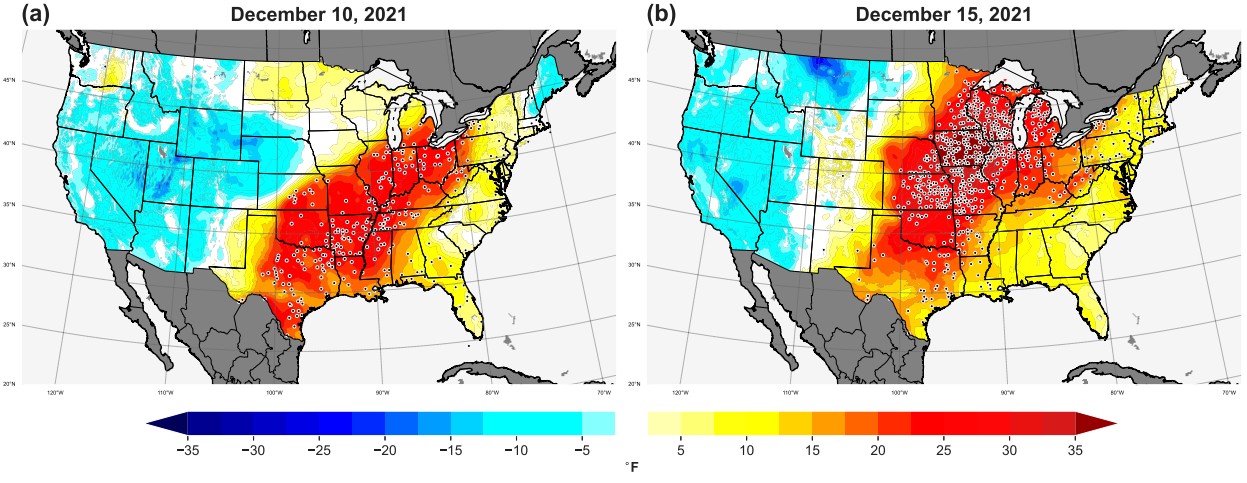

FIG. 5. NOAA daily U.S. climate gridded dataset (nClimGrid; Durre et al. 2022) daily maximum temperature anomalies (°F) for (a) 10 Dec and (b) 15 Dec. Anomalies are computed relative to a 31-day mean centered on each calendar day for the 1991–2020 climatological period. The black circles represent surface observation stations which set a new daily record for maximum temperature.

coverage, with total severe PPH exceeding 30%. Deeper upper-level troughing in the western CONUS began to materialize by 9 December, as the northern and southern stream troughs, evident on 8 December, began to phase, favoring cyclogenesis east of the Rockies (Gaza and Bosart 1990). The anomalous trough and cyclogenesis on 10 December set the stage for the first tornado outbreak. As the trough progressed eastward on 11 December, the severe threat evolved toward primarily a wind risk (not shown). A substantial central U.S. upper-level ridge persisted on 12–14 December before the next western trough ejected eastward, and lee cyclogenesis ensued on 15 December, promoting the derecho and tornado outbreak across the central Plains into the Midwest. As 10 and 15 December were significant severe weather outbreaks, and combined for 83% of the total December 2021 tornadoes, they will be the events of focus for the remainder of the manuscript given their impact.

Throughout November 2021, sea surface temperature (SST) anomalies in the Gulf of America/Gulf of Mexico[1] (GoM) averaged 0.77°C above the 1991–2020 mean, with a significant warming trend observed during the first 2 weeks of December 2021. By 10–15 December, SST anomalies approached 1.5°C (Fig. 2). The persistent 500-hPa ridging over the GoM through the first half of December contributed to

[1] On 20 January 2025, President Trump issued an Executive Order that renamed the portion of the Gulf of Mexico within the U.S. Exclusive Economic Zone as the "Gulf of America." Therefore, U.S. government agencies refer to this body of water as the "Gulf of America/Gulf of Mexico" when information in scientific products from this region is referenced beyond the United States. Use of "nameA/nameB" follows customary practices of cartography when countries sharing a given geographical feature do not use a common name.

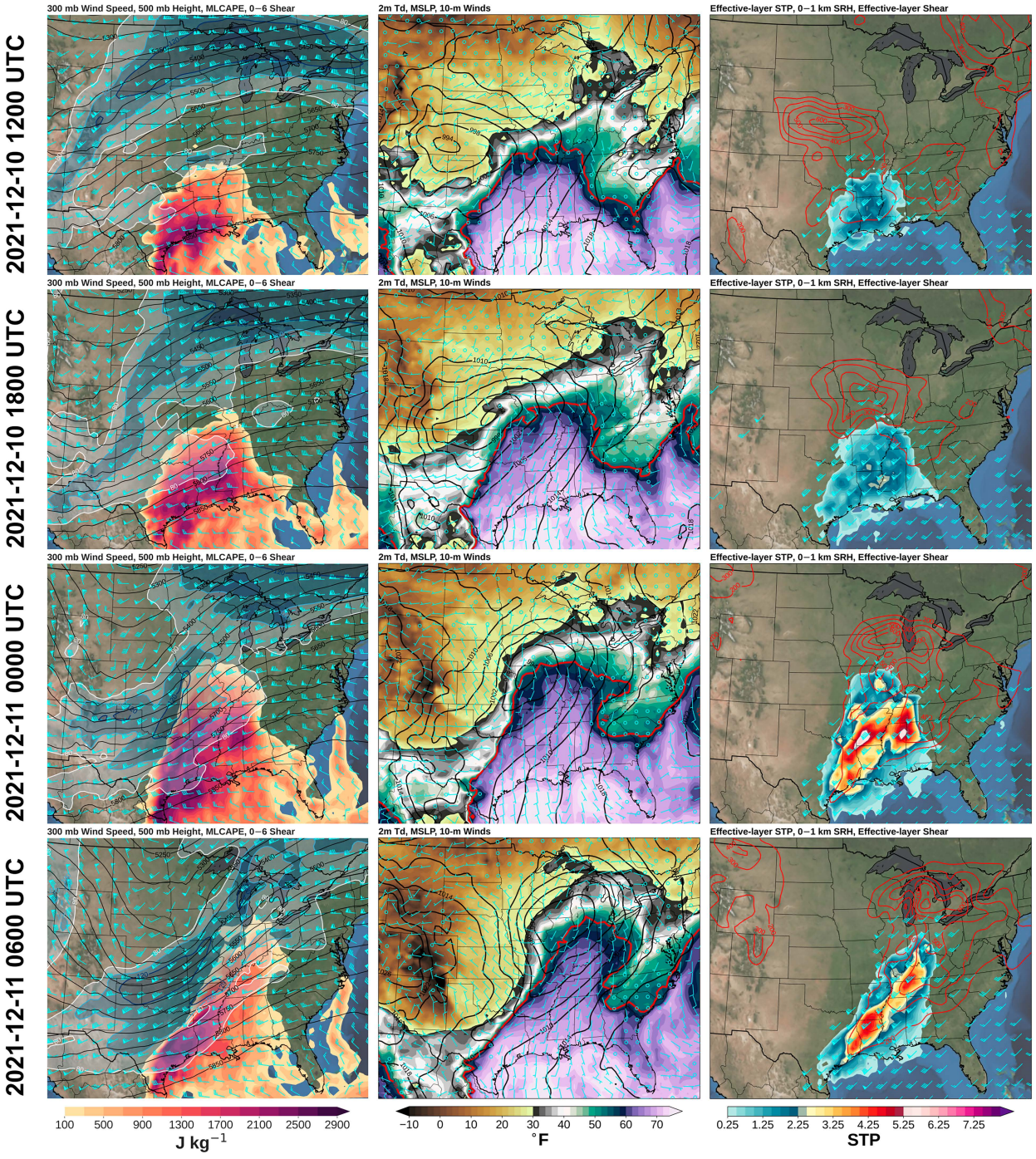

FIG. 6. The 6-hourly synoptic-scale evolution from 1200 UTC 10 Dec 2021 to 0600 UTC 11 Dec 2021 (left) 300-hPa wind speed (kt; translucent blue shading every 10 kt beginning at 80 kt), 500-hPa geopotential height (gpm; black contours), 100-hPa MLCAPE (J kg^{-1}), and 0–6-km shear vectors (kt; cyan barbs); (center) 2-m dewpoint temperature (°F), 55°F isodrosotherm (red contour), mean sea level pressure [mb (1 hPa = 1 mb)], and 10-m winds (kt; barbs); and (right) effective-layer STP, effective-layer shear vectors (kt; cyan barbs), and 0–1-km SRH (m s^{-1}; red contours).

warming SSTs via inferred large-scale subsidence and increased insolation (Fig. 1). In addition, ridging over the central CONUS through the first week of December was unfavorable for cold fronts to surge southward across the GoM. Passage of cold fronts across the GoM can reduce SSTs via upwelling and convective mixing while also impeding the return flow from the GoM as cold air filters to lower latitudes (Hsu 1997; Villanueva et al. 2010; Zavala-Hidalgo et al. 2014; Wang et al. 2023;

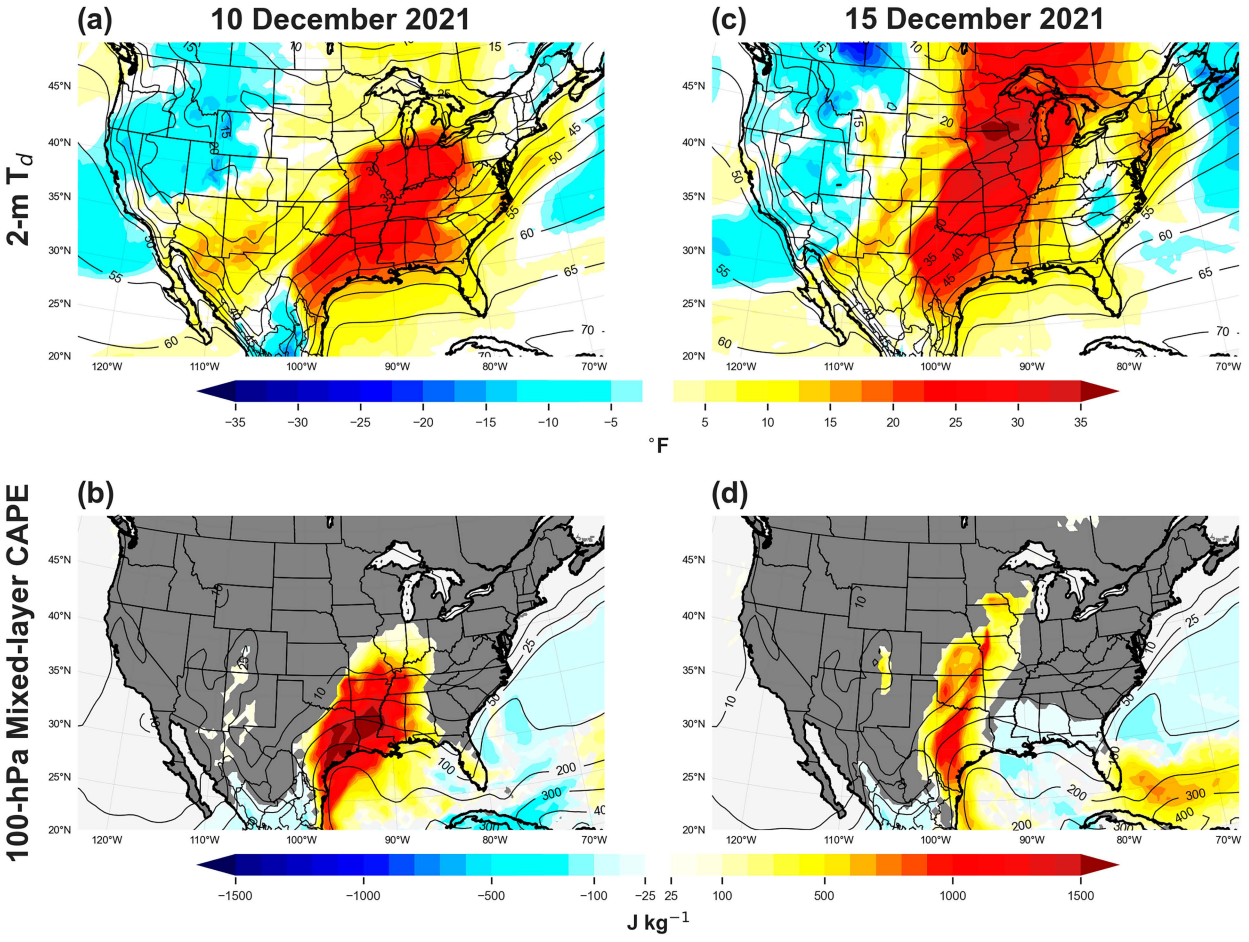

FIG. 7. Daily (1200–1200 UTC) maximum dewpoint temperature anomalies (color filled; °F) and climatological mean (contoured) from GEFS ANL for (a) 10 Dec and (c) 15 Dec, and daily maximum MLCAPE anomalies for (b) 10 Dec and (d) 15 Dec. Anomalies are computed relative to the daily (31-day centered) 2000–19 climatological mean.

Crisp and Lewis 1992). Consequently, a warm GoM was "open" for poleward advection of warm, moist boundary layer air into the CONUS (Lewis et al. 1989). The GoM serves as a crucial moisture source for severe weather, particularly in the cool season, by increasing surface dewpoint temperature and enhancing convective instability in the warm sector of extratropical cyclones (Lewis et al. 1989; Weiss 1992; Molina et al. 2016, 2018; Molina and Allen 2019, 2020; Molina et al. 2020).

2) 10 DECEMBER 2021

The Storm Prediction Center issued a moderate risk for severe thunderstorms, highlighting a threat of significant tornadoes and widespread damaging wind gusts, in day 1 convective outlook issued at 1630 UTC (Fig. 3a). Two primary corridors of tornadic storms were observed on 10 December 2021 (Fig. 4a). The northern portion of the outbreak produced tornadoes predominantly in Missouri and Illinois, with two EF3 tornadoes near St. Louis, Missouri. On the east side of St. Louis, across the Mississippi River in Illinois, a relatively short-lived EF-3 tornado struck an Amazon distribution center in Edwardsville, Illinois, resulting in six fatalities from the collapse of the structure (SPC 2024; Maruf 2021). The supercell that produced these tornadoes produced several more tornadoes, including two EF2 tornadoes in central Illinois. In the second corridor further to the southeast in Arkansas, Tennessee, and Kentucky, unfortunately, a more devastating scenario occurred with multiple long-track violent tornadoes. A single long-lived (~11 h) tornadic supercell thunderstorm (the "quad-state supercell"; Guyer 2022; Van Den Broeke et al. 2023) traveled ≈ 750 km from northeast Arkansas until its dissipation in northern Kentucky, producing 11 total tornadoes, including two long-track violent EF4 tornadoes responsible for 67 fatalities (Fig. 4a). The supercell circulation was briefly disrupted by interaction with another storm in northwest Tennessee, precluding a continuous tornado path of the two EF4 tornadoes (Van Den Broeke et al. 2023). Additional long-track tornadoes occurred further to the south and east. After the event, tornado scars were observed from observations from the

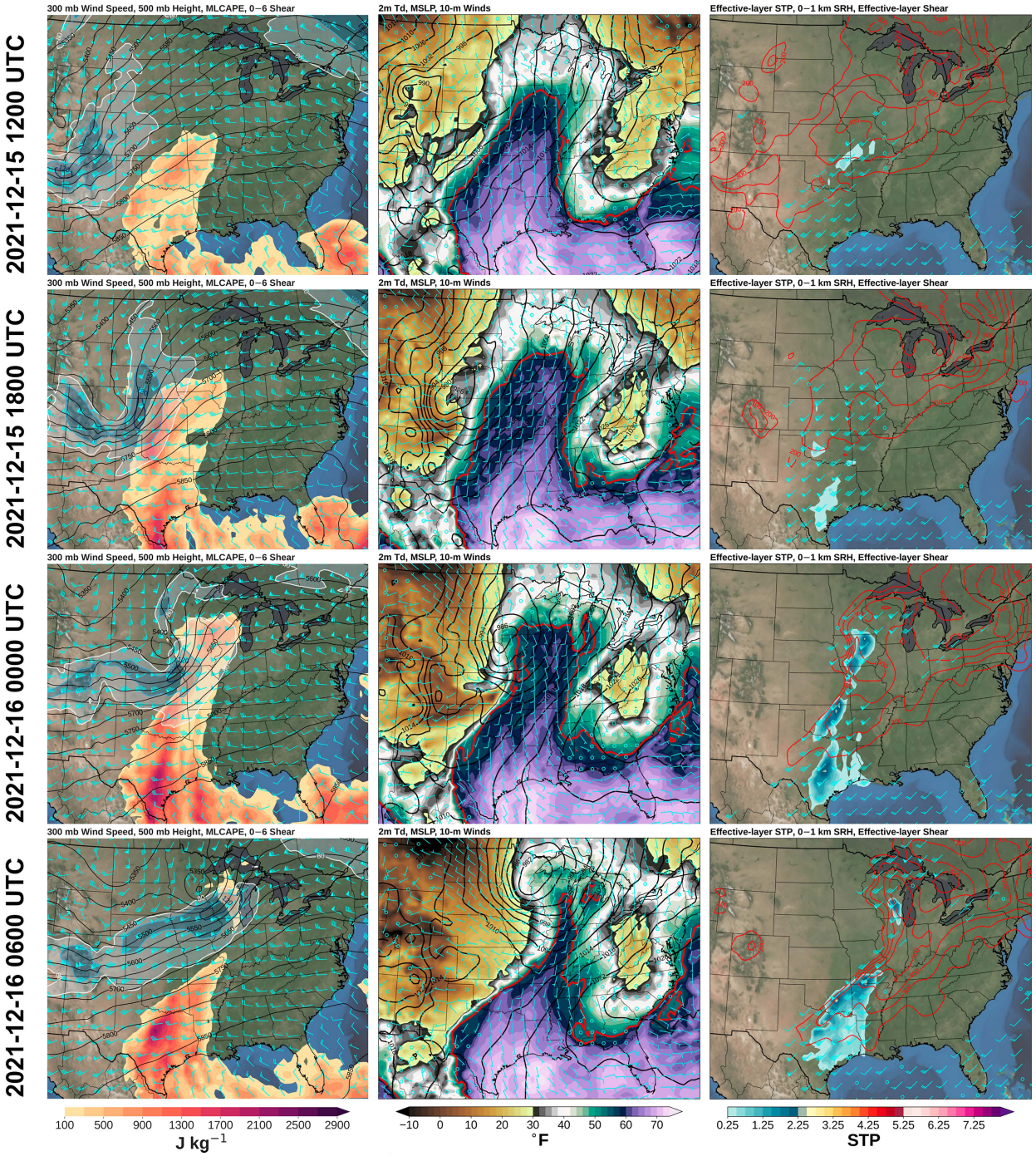

FIG. 8. As in Fig. 6, but for the period between 1200 UTC 15 Dec and 0600 UTC 16 Dec 2021.

shortwave infrared channels of the Moderate Resolution Imaging Spectroradiometer (MODIS) (Wang et al. 2023).

Unseasonably warm conditions were in place for 10 December 2021, characterized by a corridor from the southern Great Plains northeast to the Midwest that exhibited maximum temperatures 20°–25°F above normal (Fig. 5a). A surface low pressure system developed at 1200 UTC in eastern Colorado ahead of a trough at 500 hPa and in the equatorward entrance region of an upper-level jet at 300 hPa (Fig. 6). As the surface cyclone moved east-northeastward through 0000 UTC 11 December, warm, moist air was rapidly advected northward from the GoM. Dewpoint temperatures in central and southern Illinois, initially in the 30°–50°F range at 1200 UTC, increased into the upper 50s and lower 60s (°F) by 0000 UTC 11 December with the passage

of a northward-moving warm front (Fig. 6). Similarly, unseasonable moisture surged northward into the lower Ohio River valley promoting the development of moderate 100-hPa mixed-layer convective available potential energy (MLCAPE). Given the time of year, the degree of moisture and instability was highly anomalous (Figs. 7a,b). With strong 0–6-km vertical wind shear, a very favorable parameter space was in place for the development of supercell thunderstorms (Fig. 6). As the low-level jet strengthened into the evening and overnight hours, low-level shear and storm-relative helicity (SRH) increased, with 0–1-km SRH values exceeding 400 $m^2 s^{-2}$ in Kentucky by 0600 11 December. Amid favorable thermodynamic and kinematic conditions, the effective-layer significant tornado parameter (STP; Thompson et al. 2012) increased by 0000 UTC in both tornado corridors, with values exceeding 1 indicative of an environment supportive of significant tornadoes (see the appendix for STP formulation). The persistence of highly favorable conditions supported the nocturnal tornadoes, which are known to be disproportionately more deadly than their daytime counterparts (Ashley et al. 2008; Strader et al. 2022).

3) 15 DECEMBER 2021

A serial derecho and tornado outbreak occurred in the upper Midwest on 15 December. Although the upper Midwest experiences derechos, they are nearly exclusively confined to the warm season (e.g., Guastini and Bosart 2016). In terms of the annual cycle, derecho occurrence is minimized during the cool season, and they are most infrequent during the month of December; when they do occur, they are typically confined to the southeast United States (Squitieri et al. 2023, and references within). The SPC highlighted the threat of widespread significant wind gusts and the potential for a few tornadoes, driving a categorical moderate risk in their day 1 convective outlook product (Fig. 3e). Convection began along the cold front in north central Kansas and quickly became severe by 1900 UTC and produced severe weather for ~10 h as the quasi-linear convective system (QLCS) advanced rapidly northeastward (not shown). Tornadoes were produced at the leading edge of the QLCS among a broad corridor of widespread significant severe wind damage from convective wind gusts (Fig. 3f). Iowa set a new record for daily tornadoes (63), surpassing the previous maximum of five for December (SPC 2024) (Fig. 4b). Additionally, it was also the first time a tornado occurred in Minnesota during the month of December. The anomalous number of tornadoes produced by the derecho aligns with the documented increase in the number of tornadoes associated with QLCSs, although the causality of the trend is still uncertain (Thompson 2023).

A negatively tilted and compact upper-level shortwave trough accompanied by a strong (>60 m s^{-1}) jet stream at 300 hPa contributed to lee cyclogenesis over eastern Colorado by 1800 UTC that rapidly deepened as it tracked north-northeast (Fig. 8). Anomalously warm conditions were in place throughout much of the eastern CONUS, with a large region in the Midwest, from northern Missouri to southeast Minnesota and Wisconsin, recording daily maximum temperatures more than

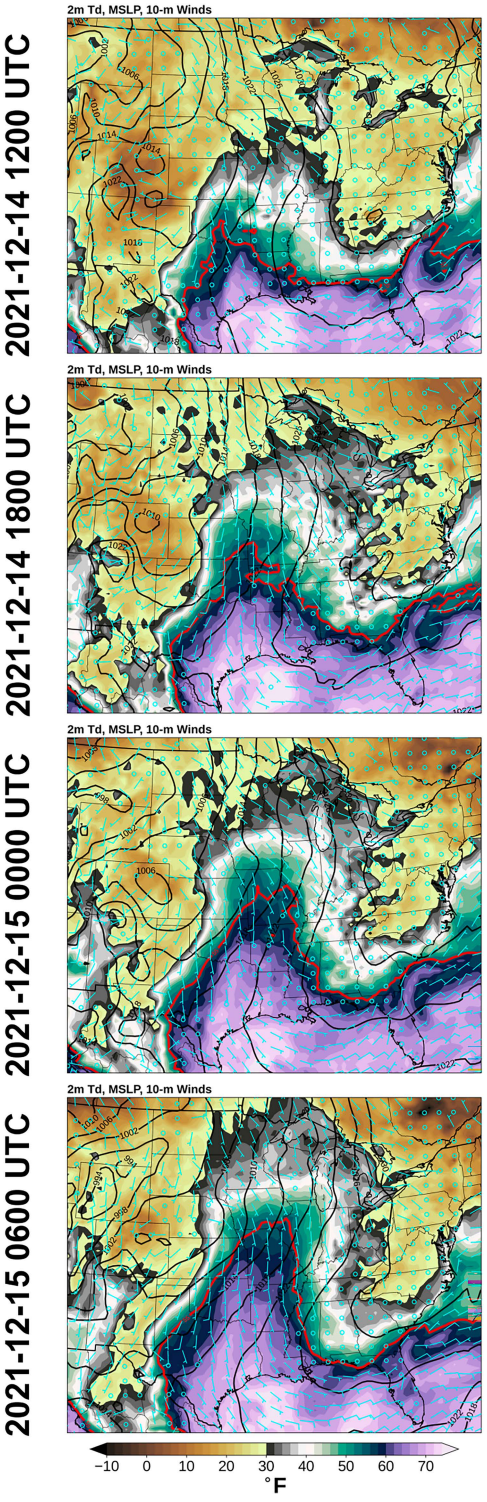

FIG. 9. The 2-m dewpoint temperature (°F), 55°F isodrosotherm (red contour), mean sea level pressure (mb), and 10-m winds (kt; barbs) for the period between 1200 UTC 14 Dec and 0600 UTC 15 Dec 2021.

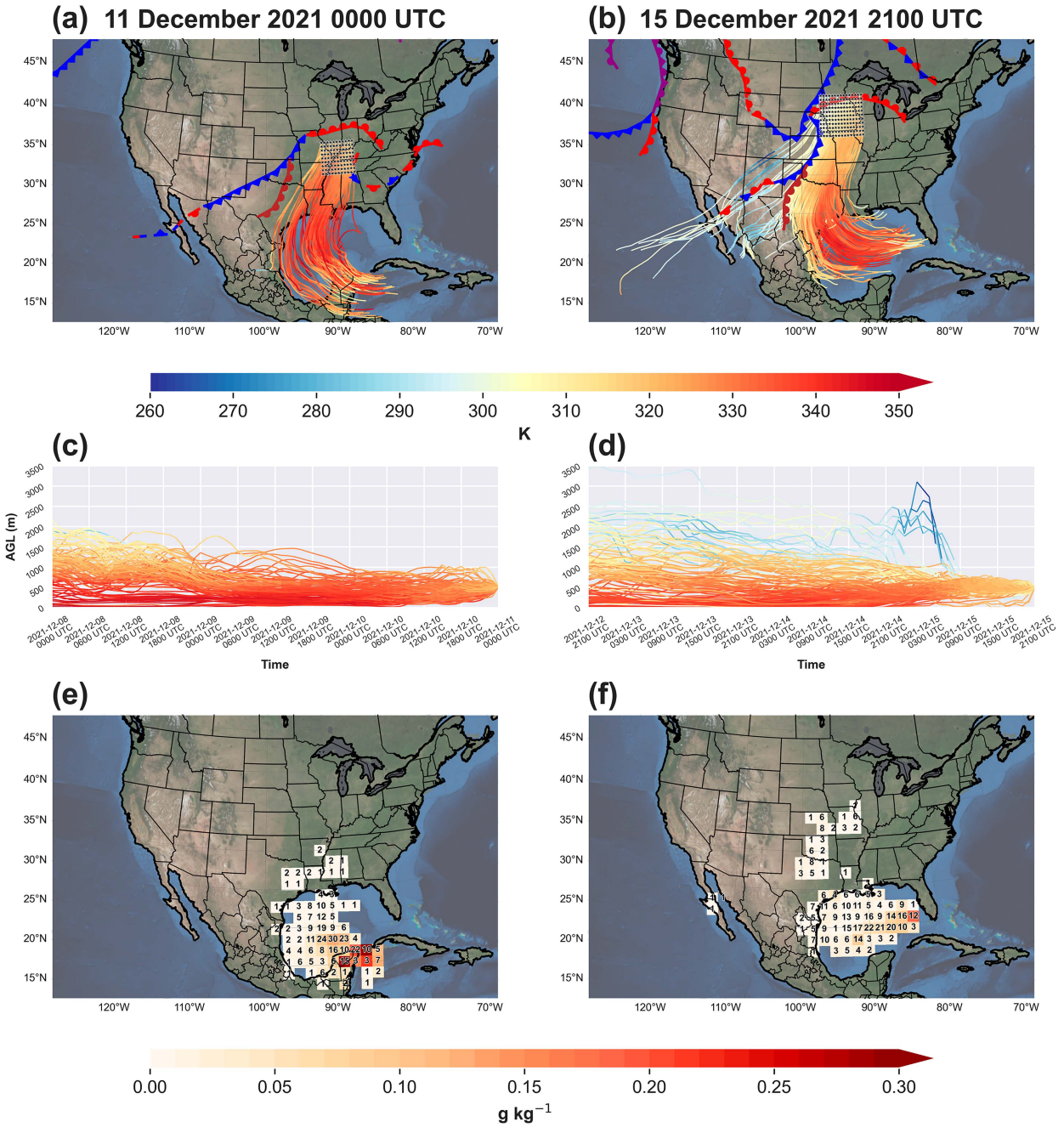

FIG. 10. The 72-h backward HYSPLIT trajectories initialized at (left) 0000 UTC 11 Dec and (right) 2100 UTC 15 Dec 2021. (a),(b) WPC analyzed surface fronts and drylines and 72-h backward HYSPLIT trajectories with an initial source height of 500 m. The trajectories are colored by equivalent potential temperature θ_e (K). (c),(d) The elevation (m AGL) and θ_e of each parcel trajectory are plotted through time. (e),(f) Frequency-weighted MU locations and amounts (specific humidity) with the total number of MU trajectories passing through each grid box annotated.

30°F above average with over 700 surface observation stations set a new daily record for high temperature (Fig. 5b). The northward extent of warm and moist conditions was very unusual for December, with dewpoint temperatures exceeding 55°F as far north as southeastern Minnesota, central Wisconsin, and into southwestern Lower Michigan. Strong poleward water vapor advection in the central Plains began the previous day, allowing for 30°–40°F rise in dewpoint temperatures in less than 24 h (Fig. 9), contributing to MLCAPE values between 750 and 1000 J kg^{-1} by 0000 UTC 16 December ahead of the northeastward advancing derecho (Fig. 8). Climatologically, the moist, unstable conditions in the central CONUS,

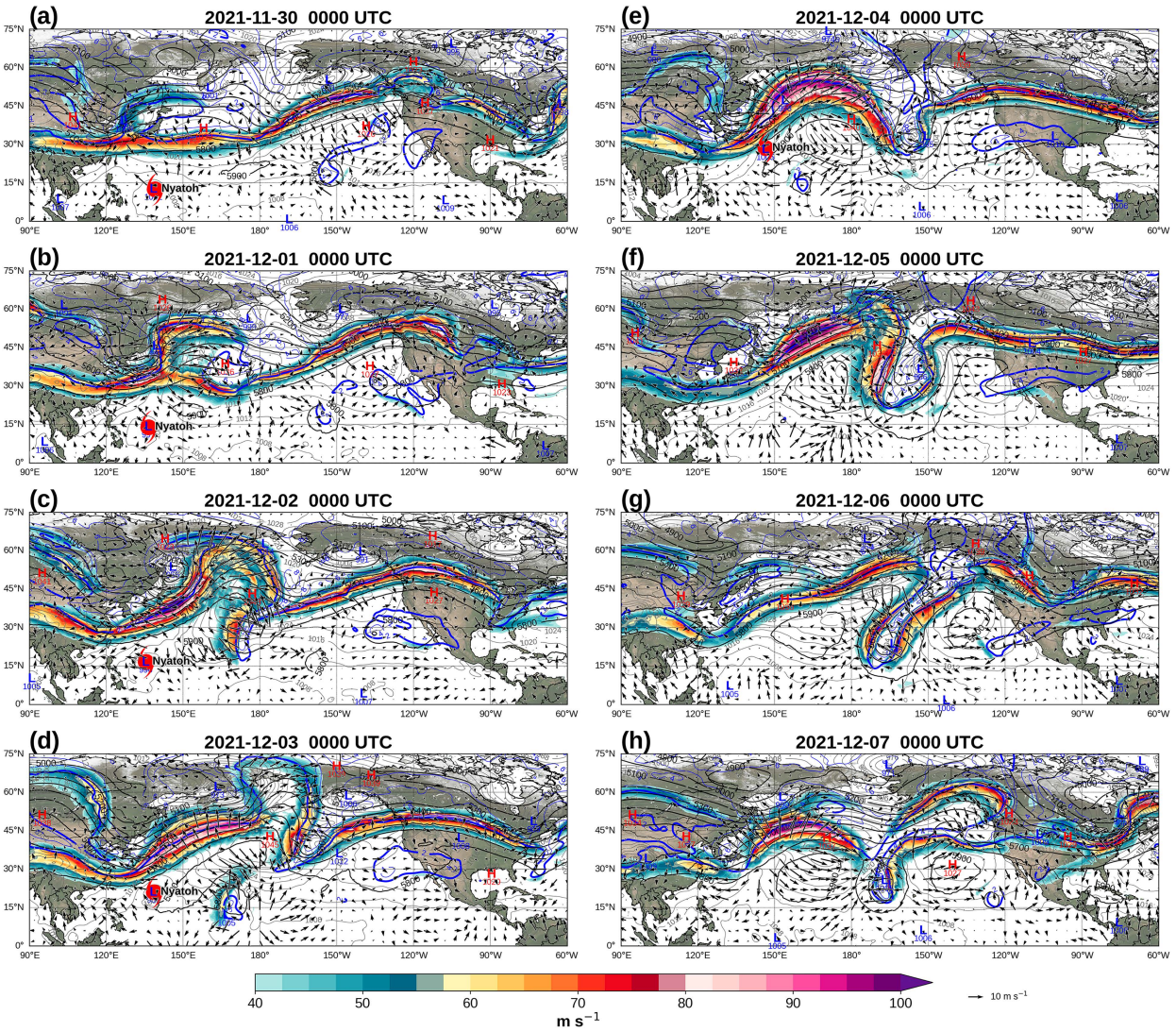

FIG. 11. Progression of the Northern Hemisphere flow between 0000 UTC 30 Nov and 0000 UTC 6 Dec as illustrated by 250-hPa wind speed (m s^{-1}; color filled), irrotational wind vectors (m s^{-1}), and PV (every 2 PVU; blue contour), 500-hPa geopotential height (m), and mean sea level pressure (mb; black contours). High and low pressure centers are labeled with red H and blue L, respectively. The reference vector for the irrotational winds is displayed to the right of the color bar. The central position of Typhoon Nyatoh is represented by the red TC symbol.

particularly their northward extent, were significantly anomalous (Figs. 7c,d).

b. *Moisture attribution*

Warm GoM SSTs contribute to moist and unstable conditions that favor severe weather outbreaks (Molina and Allen 2019; Molina et al. 2020). Given the anomalously warm, moist, and unstable conditions present during the 10 and 15 December severe weather events (Figs. 5 and 7) in conjunction with above-average GoM SSTs (Fig. 2), here we explore the role of GoM SSTs more quantitatively via 72-h backward trajectory analyses. The trajectories were initiated over the primary outbreak regions at a time preceding the onset of severe storms for each event in an effort to sample the preconvective environment in which storms would move into (Figs. 10a,b). For the 10 December event, air parcels in the previous 3 days are shown to have originated primarily from the western Caribbean Sea, before crossing northwestward across the Yucatán Peninsula into the western GoM. Parcels increased their equivalent potential temperature θ_e during the day on 9 December over the western GoM (and descended to lower altitudes) before being advected northeastward from the western GoM into the warm sector of the surface cyclone (Figs. 10a–c). In terms of MU, 95% of all trajectory uptake points occurred over GoM and northwestern Caribbean (Fig. 10e).

In contrast with 10 December, the trajectory analysis for the 15 December event found that the majority of parcels

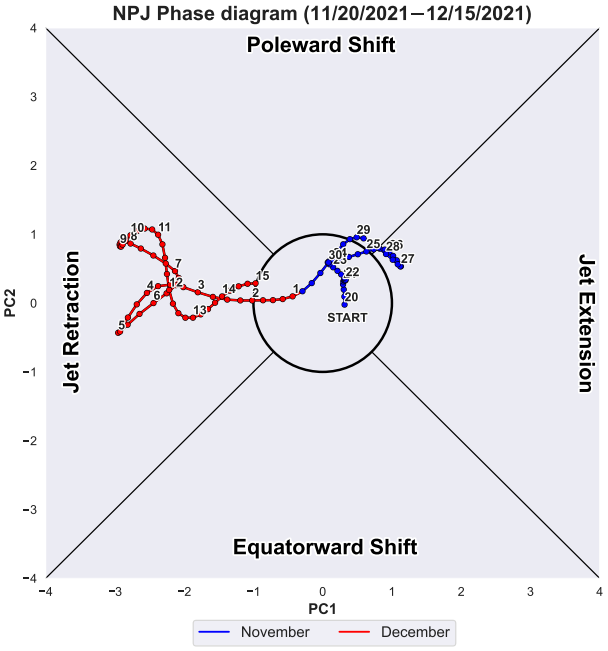

FIG. 12. The NPJ phase diagram valid between 20 Nov and 15 Dec 2021.

within the warm sector originated within the GoM and the eastern GoM in particular (Fig. 10b). The lower θ_e air parcels which originated over the Pacific Ocean, Baja California, and northern Mexico were primarily associated with airflow on the backside of the surface cyclone and initial trajectory locations along the cold front or north of the warm front. The highest θ_e parcels originated over the central and western GoM, with ~81% of trajectory MU points occurring over the GoM basin (Fig. 10e).

Overall, these results are in line with previous research that demonstrated that cool-season tornado events primarily derive moisture contributions from the GoM and the northwestern Caribbean Sea (Molina and Allen 2019; Molina et al. 2020).

c. *Upstream antecedent conditions over the North Pacific*

The synoptic conditions favoring CONUS severe weather frequency during the study period can be linked upstream to multiscale processes over the Pacific Ocean and their subsequent impact on the evolution of the jet stream structure over the North Pacific. Of particular interest are 1) the extratropical cyclogenesis (ETC) on 30 November off the east coast of Asia, 2) the interaction of Typhoon Nyatoh with the North Pacific jet stream, and 3) subsequent ETC occurrences on 7 and 11 December west of the international date line (IDL). An upper-level trough over East Asia aided an explosive coastal extratropical cyclogenesis event on 30 November over the Sea of Japan (Fig. 11a). This cyclone rapidly deepened from 1009 to 955 hPa in the 48 h between 0000 UTC 30 November and 0000 UTC 2 December 2021 (Figs. 11a–c). This event significantly transported poleward momentum, increased downstream geopotential height, developed a >100 m s^{-1} jet streak at 250 hPa, and caused anticyclonic Rossby wave breaking near the IDL by 0000 UTC 2 December—evidenced by the reversal in the meridional 250-hPa PV gradient between 30° and 50°N (Fig. 11c). This initial event amplified the flow downstream across the North Pacific and evolved the NPJ to a retracted regime (Fig. 12). The cyclogenesis event also triggered the first RWP in December 2021, which is clearly illustrated in a Hovmöller diagram of the anomaly of the daily mean 35°–55°N v-wind component at the dynamic tropopause, defined by the 2-PVU surface (1 PVU = 10^{-6} K kg^{-1} m^2 s^{-1}) (Fig. 13). The RWP enhanced downstream amplification across the North Pacific and shifted the trough position in North America westward to around 90°W by 5 December (Figs. 1 and 11f,g). This westward shift in the upper-level trough in North America set the stage for the severe weather events on 5–6 December.

Typhoon Nyatoh began as a tropical disturbance on 28 November and strengthened to a tropical storm by 1800 UTC 29 November (Fig. 14). Upon poleward recurvature on 2 December, Nyatoh underwent rapid intensification to a category 4 supertyphoon, reaching peak wind speeds of 66 m s^{-1} and a minimum central pressure of 928 hPa by 2100 UTC 2 December. Nyatoh underwent an extratropical transition at 0000 UTC 4 December before rapidly dissipating. While recurving, Nyatoh began to interact with the NPJ, with maximum interaction occurring at 0000 UTC 3 December (Fig. 15). To quantify the strength of the interaction, the TC interaction metric was derived from GEFS ANL, with a final value of −3.41 PVU day^{-1}, indicative of a strong interaction between the divergent outflow from the TC and the jet-level PV gradient. As in Archambault et al. (2013), the relative location of the maximum interaction was confirmed to be within the vicinity of the TC cirrus shield. The calculation was repeated using the 2.5° × 2.5° NCEP–NCAR reanalysis data (Kalnay et al. 1996) to compare with the climatology results of Archambault et al. (2013), and the resulting value of −2.79 PVU day^{-1} places Nyatoh as the strongest TC interaction relative to those examined by Archambault et al. (2013) during the period 1979–2009.

Negative PV advection by the irrotational wind along the axis of the PV waveguide and upper-level jet increased as TC Nyatoh approached the region on 2–3 December (Figs. 16a–e). In addition to strengthening and anchoring the southwest end of the upper-level jet near 30°N, 135°E, the downstream ridge amplified just west of the IDL by 0000 UTC 4 December (Figs. 16f–i). The negative PV advection by the irrotational wind was associated with deep convection near TC Nyatoh's center and a southwest-to-northeast oriented region deep convection and attendant irrotational outflow that extended to the northeast of Nyatoh. To isolate the contribution of irrotational outflow from these features, the TC interaction metric was recomputed with the irrotational wind associated with divergence within 10° of TC Nyatoh's center removed using the divergence inversion technique. The resulting TC interaction metric with the effects of TC Nyatoh removed was found to be −2.47 PVU day^{-1}, a ~28% reduction in the magnitude of the interaction metric, thus highlighting the importance of TC

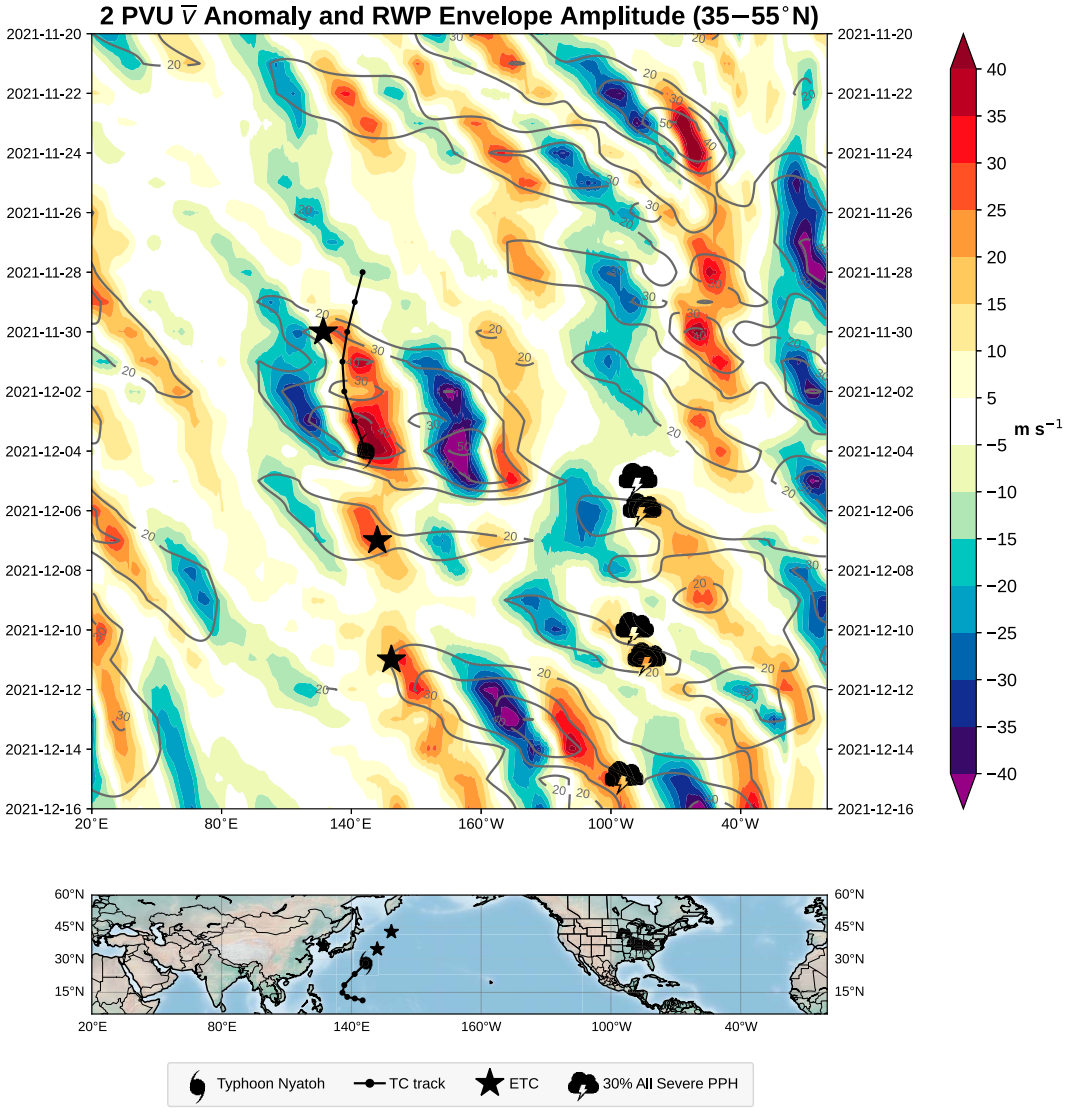

FIG. 13. (top) Hovmöller diagram of the daily mean V-wind anomaly on the 2-PVU surface. Gray contours represent the RWP envelope magnitude (e.g., Zimin et al. 2006) greater than 20 m s^{-1} and (bottom) map denoting the geographic location of relative features. The location of Typhoon Nyatoh, notable ETC locations, and the centroid of severe weather locations are annotated.

Nyatoh in the strengthening and anchoring of the upper-level jet and subsequent downstream amplification.

The band of deep convection extending northeast from TC Nyatoh developed as a plume of deep tropical moisture, with total column precipitable water values over 60 mm, was transported northward ahead of Nyatoh (Fig. 17). This poleward water vapor transport and development of deep convection suggests the presence of a PRE, which are rainstorms that occur as deep tropical moisture is transported in advance of a TC and lifted along low-level frontal boundaries in the equatorward entrance region of an upper-level jet (Galarneau et al. 2010). PREs have been observed in midlatitudes, including North America and eastern Asia (e.g., Moore et al. 2013; Byun and Lee 2012), as well as in the subtropical North Atlantic (Galarneau 2015). In the case of TC Nyatoh, 72-h backward air parcel trajectories seeded at 3 and 5 km AGL in the PRE region show that a large portion of the air parcels originated within Nyatoh's moisture plume (Figs. 18a–c), which is a distinguishing characteristic of PREs documented in other parts of the world (e.g., Galarneau et al. 2010). Moore et al. (2013) identified three distinct synoptic-scale flow patterns associated with PREs in North America. These patterns were defined as "jet in ridge," "southwesterly jet," and "downstream confluence" and are summarized in a schematic in Moore et al. (2013) (their Fig. 20). TC Nyatoh's PRE closely resembled the "southwesterly jet" type of PRE. With this type of PRE, the combined effects of irrotational outflow from the TC and

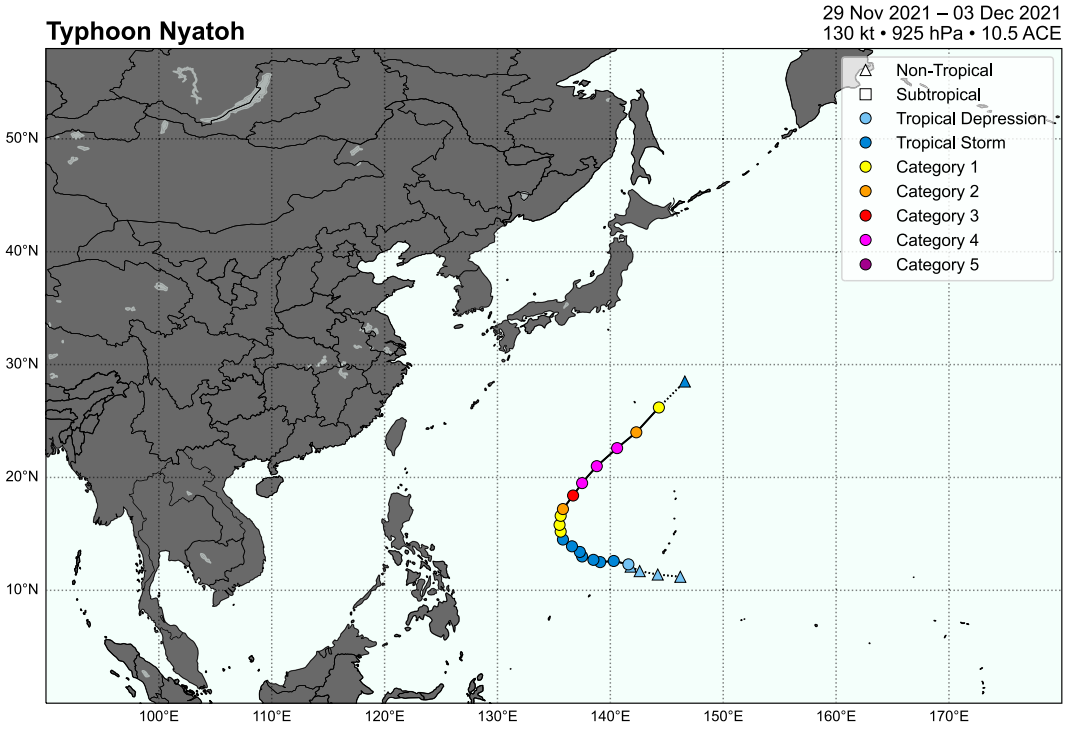

FIG. 14. Track and intensity information for Typhoon Nyatoh between 1200 UTC 28 Nov 2021 and 0000 UTC 4 Dec 2021. The plot was generated using the troPYcal Python package (Burg and Lillo 2021).

the PRE are important in upper-level jet intensification and downstream flow amplification.

As is typical of strongly interacting recurving typhoons, the strengthening of the upper-level jet streak and subsequent development of a downstream ridge following the time of maximum interaction occurred (Figs. 11e and 16f–i) (Archambault et al. 2013, 2015). By 0000 UTC 4 December, the development of an amplified ridge downstream was a textbook response. The interaction process contributed to the reinforcement of the amplified flow pattern and helped to promote the persistence of the retracted state of the NPJ (Figs. 11, 12, and 13b). The intensification of the jet streak (>100 m s^{-1}) between 150°E and 180° promoted high-latitude ETC near the IDL at ~60°N and the development of a positively tilted upper-level ridge and a digging trough by 0000 UTC 5 December in the central Pacific, leading to deepening of the surface low near 150°W (Fig. 11f). As this surface low progressed northeast, anticyclonic wave breaking (as evidenced by the meridional overturning of the 2-PVU surface at 250 hPa associated with the strongly positively tilted ridge trough pair between the IDL and 150°W) occurred by 0000 UTC 6 December and resulted in the development of a cutoff kona low near 165°W (Fig. 11g). The Kona low brought heavy rainfall and high winds to the islands of Hawaii (not shown), with impacts lasting for several days as the low slowly retrograded westward. The amplification of the ridge in the eastern North Pacific and far western CONUS modified the initial quasi-zonal jet stream over North America leading to a westward shift in the position of the upper-level trough from the western Atlantic in late November to the central and eastern CONUS, contributing to the 5–6 December 2021 severe weather events.

Another cyclogenesis event near 150°E and 38°N began by 1200 UTC 7 December (not shown) leading to intensification of the upper-level jet and development of a downstream ridge west of the IDL in conjunction with a second RWP (Figs. 13 and 19a). Anticyclonic wave breaking near the IDL contributed to the evolution of the Kona low to a westward-moving cutoff low and development of a trough just west of Baja California by 0000 UTC 9 December (Fig. 19b). A jet streak on the poleward side of the zonally elongated ridge and attendant surface cyclone reached the Gulf of Alaska, and a downstream upper-level trough developed in the western United States by 0000 UTC 10 December (Fig. 19c). The digging trough in the western United States phased with the trough near Baja California and rapidly moved eastward to the central Plains by 0000 UTC 10 December, contributing to the 10–11 December severe weather outbreak in the upper Mississippi and Ohio River valleys (Figs. 3a and 19d).

The next cyclogenesis event on 11 December near 160°E and 40°N triggered a third RWP and helped reinforce the retracted NPJ regime and downstream amplification in the north-central Pacific (Figs. 12, 13, and 19d). The surface low pressure underwent explosive cyclogenesis and was located near 50°N, 160°E by 0000 UTC 12 December. Robust irrotational outflow along the cyclone's warm front helped sharpen the PV gradient and strengthen the upper-level jet streak centered on 55°N, 165°W (Fig. 19e). Subsequent

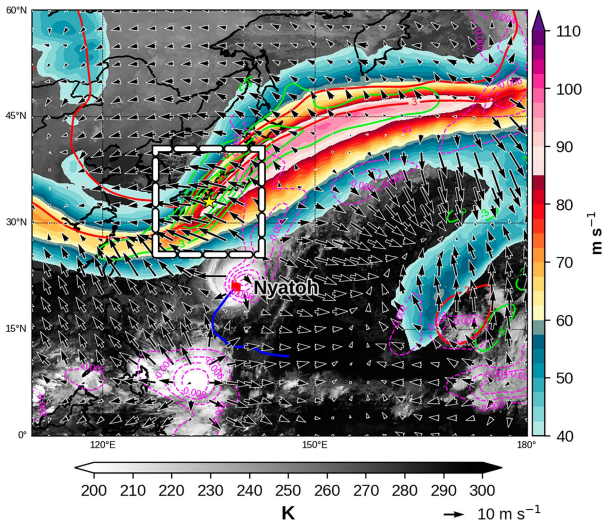

FIG. 15. Similar to Archambault et al. (2013), GEFS analyses 250–150-hPa layer mean wind speed (m s^{-1}; color filled), irrotational wind vectors (m s^{-1}), PV (red contour, every 3 PVU), PV advection by the irrotational wind (lime green contours; every −3 PVU day^{-1}), mean sea level pressure (light gray contours; every 4 mb), and 500-hPa ascent (dashed magenta contours, 1×10^{-3} hPa s^{-1}) are plotted at the time of maximum TC–extratropical flow interaction associated with Typhoon Nyatoh (0000 UTC 3 Dec 2021). GridSat (Knapp et al. 2010) geostationary infrared channel brightness temperature (K) is plotted, and the location of the center of Typhoon Nyatoh is denoted by the red TC symbol (based on IBTrACS data), and the track up to that point is denoted by the blue line. The white dashed box represents the 15° × 15° latitude–longitude box surrounding the point of minimum PV advection (denoted by yellow star) which was used to compute the TC interaction metric.

downstream amplification resulted in a meridionally elongated trough in the western CONUS, promoting explosive ETC in the central United States under a 60 m s^{-1} jet streak (Figs. 8 and 19f–h).

Overall, the evolution of the highly amplified flow pattern over the North Pacific leading up to the severe weather events was governed by a persistent retracted NPJ, a recurving TC, and frequent ETC events west of the IDL. NPJ retractions typically result in a higher amplitude/wavenumber flow pattern in the North Pacific and often lead to the development of a negative PNA pattern (Wallace and Gutzler 1981). A persistent retracted jet is also favorable for additional ETCs near the coast of East Asia and in the central North Pacific west of the IDL (e.g., Leicht and Bosart 2024). Consequently, the additional ETC events reinforced the amplified flow pattern and jet retraction, creating a positive feedback loop that allowed RWPs to propagate downstream, establishing a favorable synoptic-scale flow pattern over the CONUS for the 10 and 15 December outbreaks. Ultimately, these processes caused a westward phase shift of the eastern CONUS upper-level trough, enhancing favorable conditions for severe convective storm development (Fig. 13).

5. Discussion

The explosive cyclogenesis event off the East Asian coast on 30 November and the recurvature of Typhoon Nyatoh and subsequent strong interaction with the NPJ by 3 December, were both found to have contributed to the excitation of an RWP, resulting in retraction of the NPJ and amplification of the meridional flow downstream. This process helped shift the eastern U.S. trough, persistent through the end of November, westward which led to the favorable synoptic setup of the 5–6 December 2021 events. The subsequent persistent retracted state of the NPJ then contributed to a series of cyclogenesis events in the western North Pacific on 7 and 11 December, which helped sustain the retracted NPJ and dispersed additional RWPs downstream that maintained a highly amplified meridional flow pattern in the North Pacific. Collectively, these processes resulted in a westward phase shift of a longwave trough from the eastern to the western CONUS, leading to a more negative PNA-like pattern, which is a common response to rapid NPJ retractions. This pattern favored the movement of several shortwave troughs from the western CONUS into the Great Plains and the Mississippi River valley on 10 and 15 December 2021. In the cool season, strong dynamics accompanying weather systems are common, but in terms of severe weather potential, adequate moisture and instability are often lacking (Sherburn and Parker 2014). In this case, the persistent ridging over the Gulf of America/Gulf of Mexico during the 1–15 December period and the lack of cold fronts traversing the GoM likely contributed to anomalous warming of SSTs. Overall, the warm GoM SST anomalies played a role in providing a moisture source conducive for the development of anomalously high instability within the warm sector of the extratropical cyclones on 10 and 15 December.

As in Jiang et al. (2023), this study similarly found that the recurvature of Typhoon Nyatoh and its strong interaction with the NPJ played a significant role in maintaining the amplified flow pattern over the North Pacific and downstream. However, we find that the initial catalyst for amplification is not attributed to the TC, but rather to the explosive ETC event on 30 November off the East Asian coast. The impact of the TC recurvature and strong interaction helped to reinforce flow amplification and NPJ retraction, and the dispersion of the initial RWP downstream was not directly associated with the 10 or 15 December outbreaks. Instead, the retracted state of the NPJ favored additional ETC events west of the IDL. Although a negative PNA-like pattern was established during the week of 9–15 December, this work provides a dynamical explanation for the development of such a pattern (e.g., retracted NPJ). Consequently, the daily evolution of the 500-hPa pattern throughout the 1–15 December period of the CONUS did not reflect a typical negative PNA pattern suggested by the daily index presented by Kim et al. (2024).

While the recurvature of Typhoon Nyatoh and its interaction with the NPJ produce a textbook flow response (i.e., downstream development of an amplified ridge), to explicitly quantify the contribution of the TC to the flow amplification and predictability, vortex isolation and removal techniques ideally should be performed to confirm such an assertion.

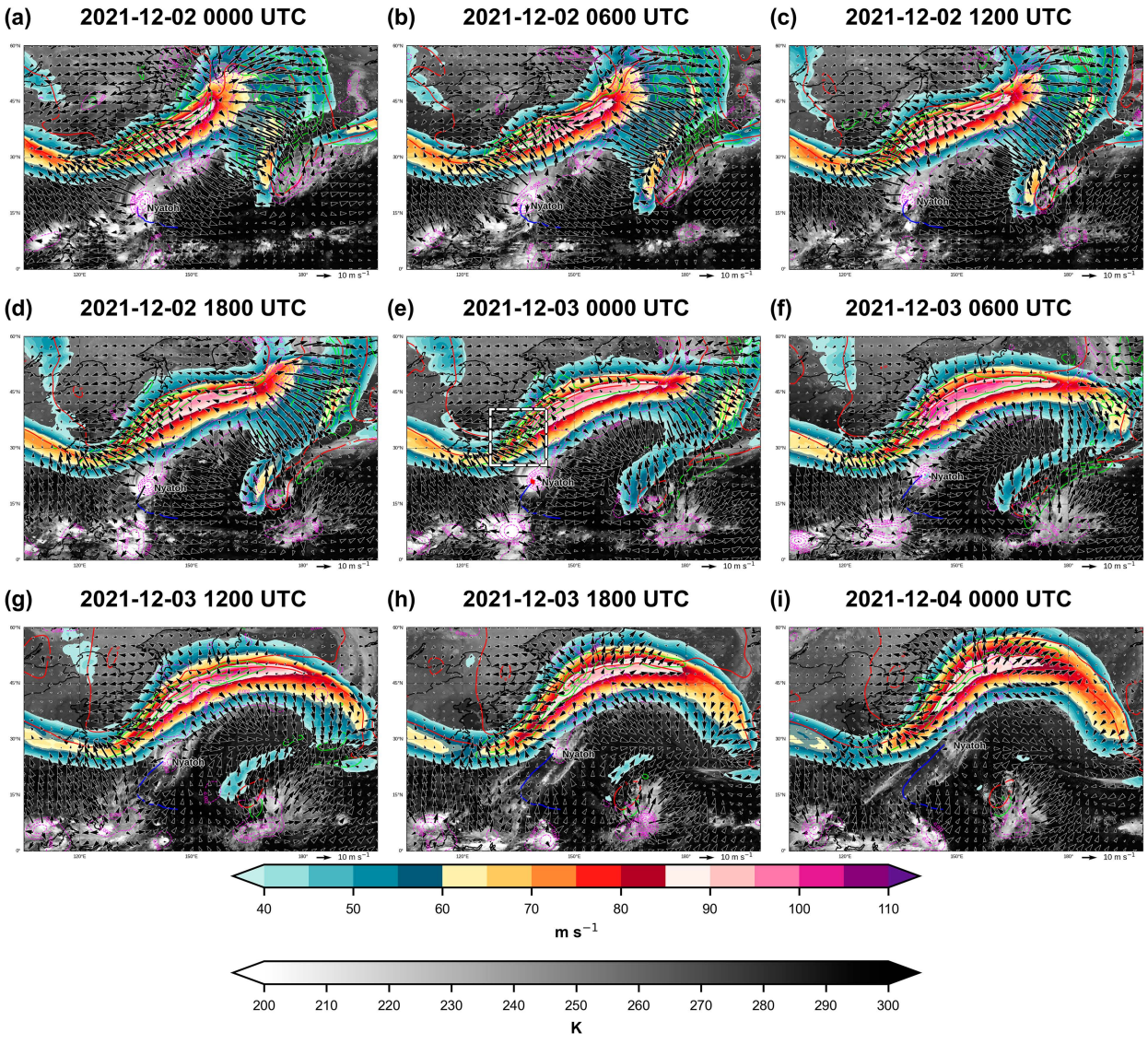

FIG. 16. As in Fig. 15, but for the 48-h period centered on the time of maximum interaction (0000 UTC 3 Dec 2021) at 6-hourly intervals.

This technique allows for a model sensitivity experiment whereby the typhoon vortex circulation can be removed, often by a PV inversion technique ("PV surgery"), to test the sensitivity of the tropical cyclone itself on the ensuing forecast (e.g., Grams et al., 2013a, 2015; McTaggart-Cowan et al. 2001, 2004). This undertaking is beyond the scope of the current study. However, through divergence inversion, we were able to assess the degree to which TC Nyatoh contributed to the total advection of PV by the irrotational wind used to compute the TC interaction metric. Removing this contribution, it was found that a weaker (nearly 30%) interaction occurred with the extratropical flow, emphasizing Typhoon Nyatoh's contributions to upper-level jet intensification and downstream flow amplification.

Given the profound impacts on downstream flow amplification due to retractions of the NPJ and recurving TCs in the western North Pacific, their recognition may provide a source of potential predictability in the medium to extended range, leading to potential forecasts of opportunity (e.g., Gensini et al. 2019; Miller et al. 2022; Miller and Gensini 2023). However, dynamical predictability within numerical weather prediction (NWP) models of the aforementioned processes is often a source of large errors in the medium range. While TC track forecasts have improved over the past few decades (Heming et al. 2019), NWP forecast skill has been shown to be highly sensitive not only to the existence of a TC, but also to its initial position, whether it undergoes recurvature, phasing and interaction with an upstream trough, extratropical transition (ET) and/or ET reintensification (Anwender et al. 2008; Grams et al. 2013b; Aiyyer 2015; Grams et al. 2015; Grams and Archambault 2016; Quinting and Jones 2016; Keller et al. 2019). Furthermore, a retracted state of the NPJ

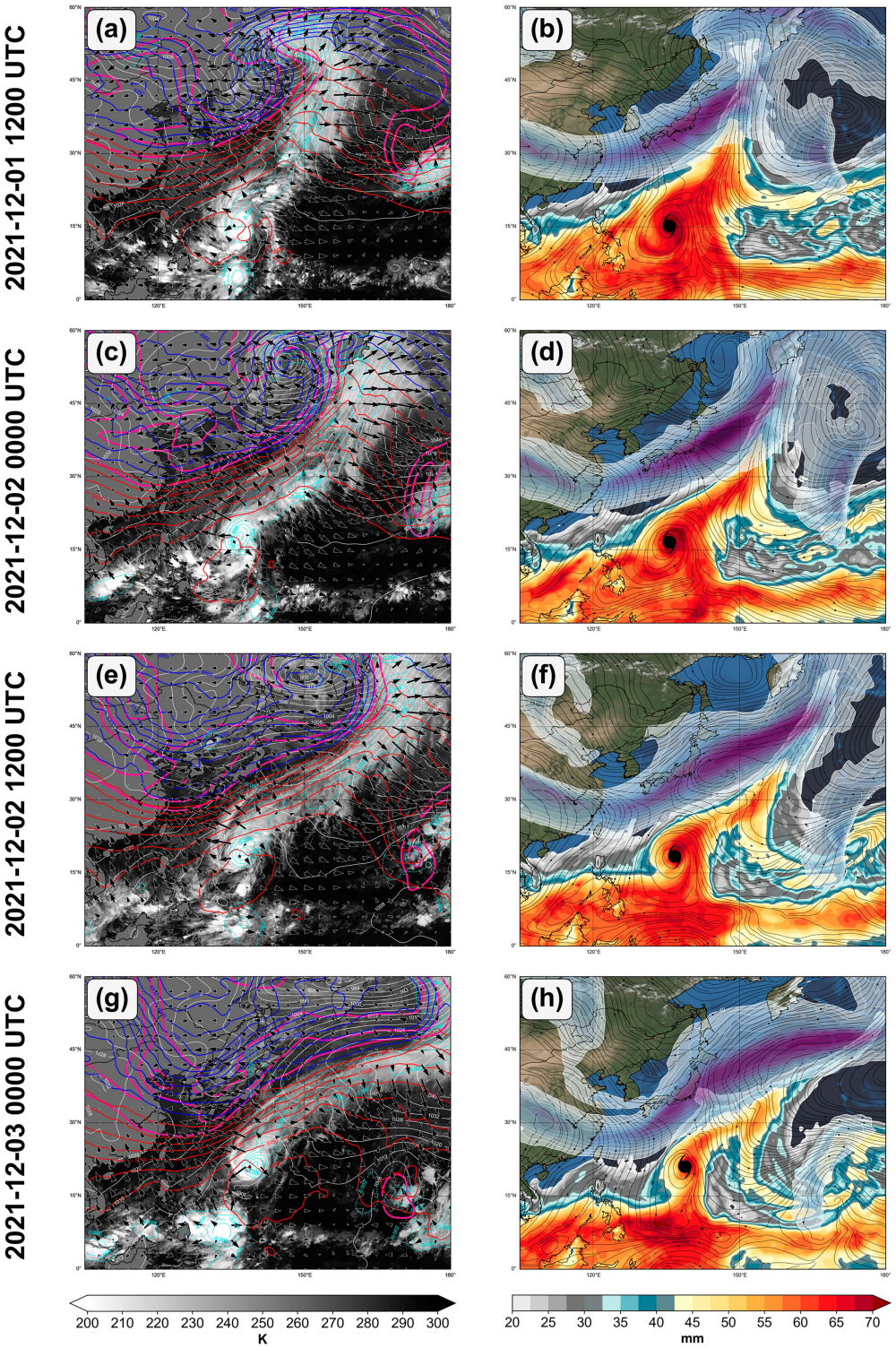

FIG. 17. (left) GridSat infrared channel brightness temperature (color filled; K), 1000–500-hPa thickness (m; red and blue contours), 2-PVU surface (pink), and 150–250-hPa layer mean irrotational winds and (right) total column integrated precipitable water (color filled; mm), 850-hPa streamlines, and 250-hPa jet stream winds greater than 40 m s^{-1} (translucent shading and contours in 5 m s^{-1} intervals), and the location of the center of Typhoon Nyatoh is denoted by the black TC symbol for (a),(b) 1200 UTC 1 Dec 2021, (c),(d) 0000 UTC 2 Dec 2021, (e),(f) 1200 UTC 2 Dec 2021, and (g),(h) 0000 UTC 3 Dec 2021.

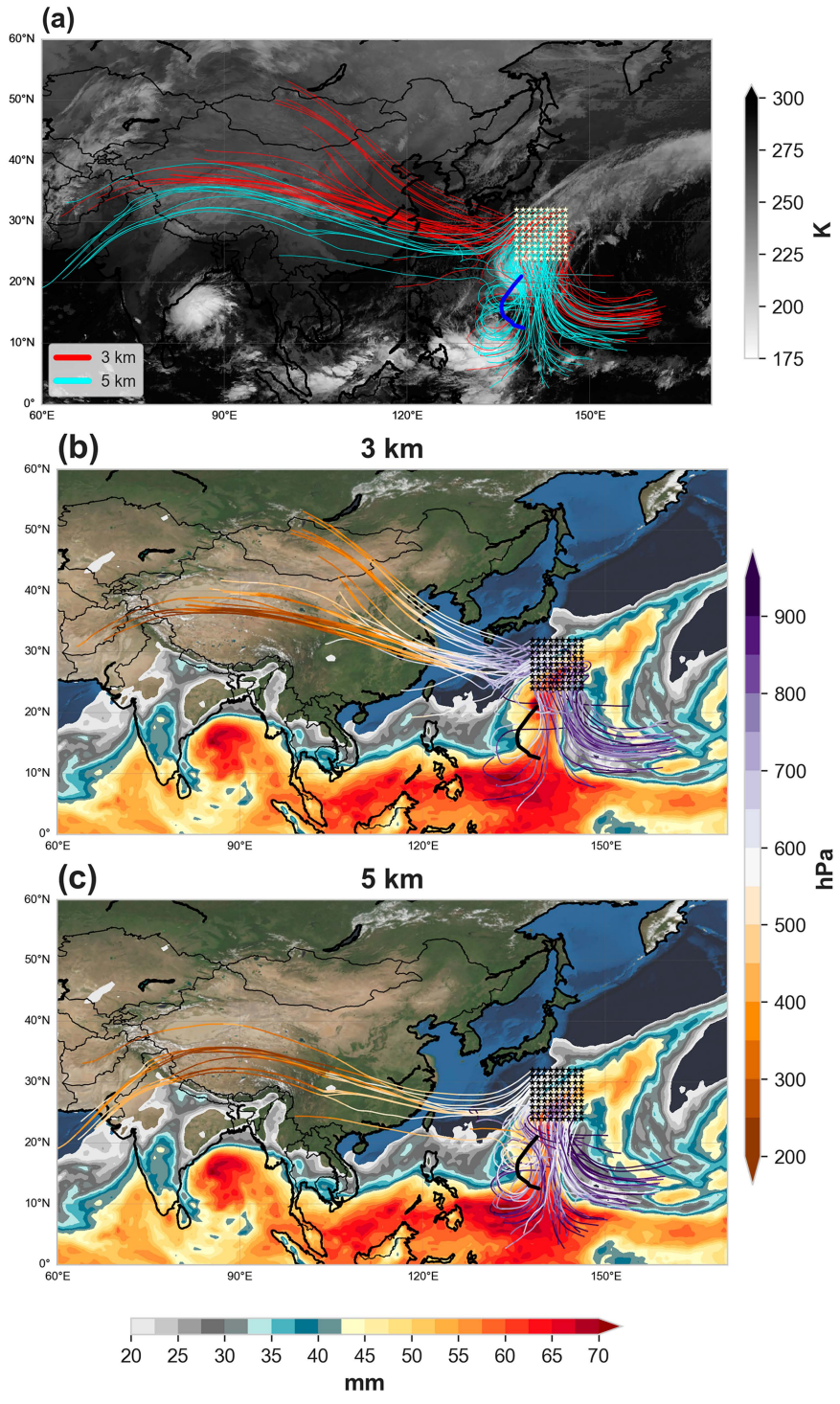

FIG. 18. (a) GridSat infrared channel brightness temperature (color filled; K) with 72-h backward trajectories initialized at 0000 UTC 3 Dec 2021 every 1° within a geographical region bounded between 20°–30°N and 135°–145°E (denoted by yellow stars) at initial altitudes of 3 (red lines) and 5 km (cyan lines) AGL. The track of TC Nyatoh is shown in blue. Total column precipitable water (mm; color-filled) with trajectory pressure level (hPa) colored lines for parcels initiated at (b) 3 and (c) 5 km.

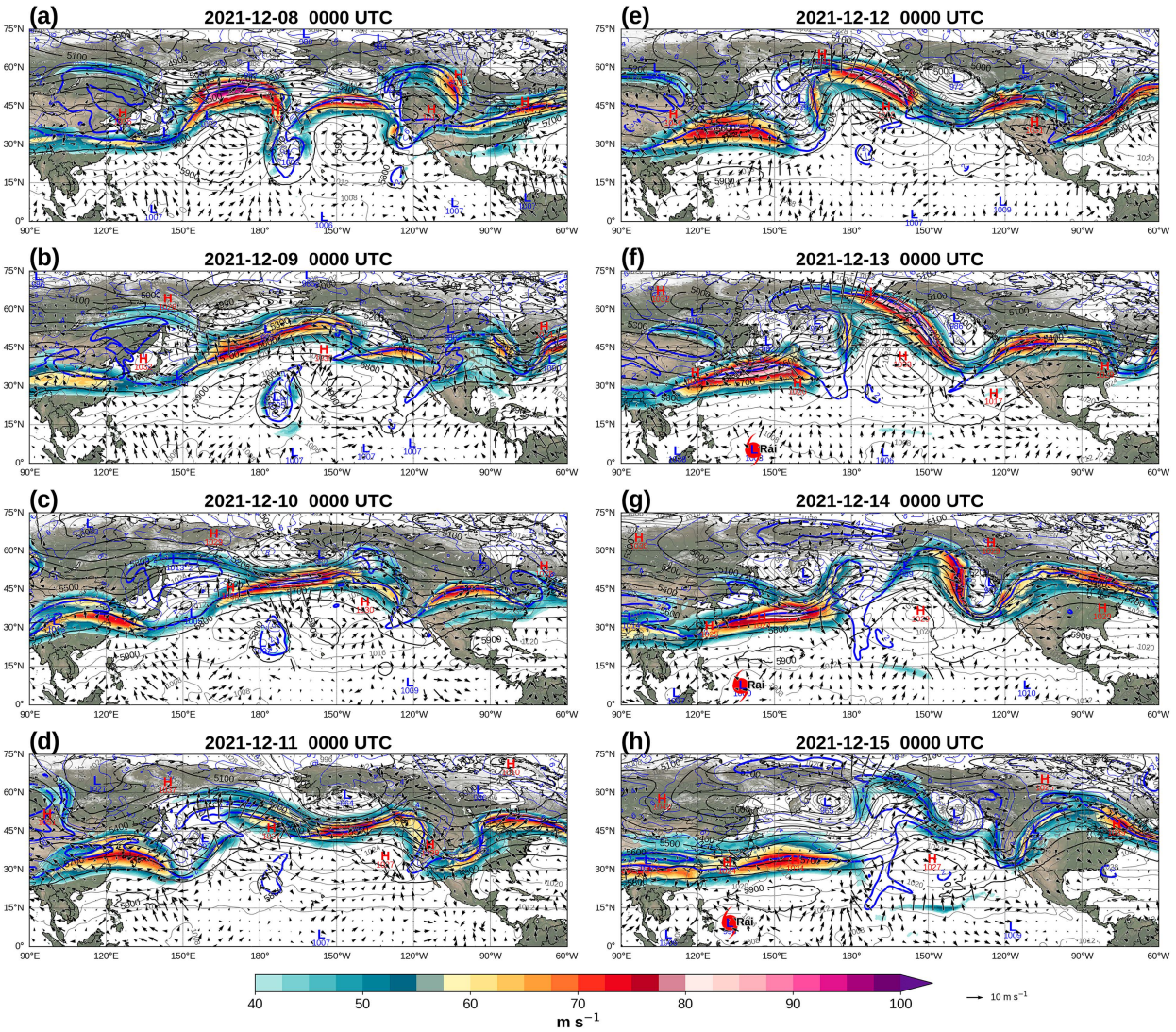

FIG. 19. As in Fig. 11, but for the period 0000 UTC 8 Dec–0000 UTC 15 Dec.

has been associated with reduced predictability within NWP forecasts due to challenges in representing the development and evolution of upper-tropospheric ridges over the North Pacific, which are often influenced by complex diabatic processes related to midlatitude cyclones and tropical convection (Winters 2021b).

6. Conclusions

The severe convective weather outbreaks on 10 and 15 December 2021 were among the most impactful December events on record, driven by a complex interaction of large-scale synoptic and mesoscale processes. This study demonstrates the importance of upstream dynamical features over the North Pacific, including explosive extratropical cyclogenesis and the recurvature of Typhoon Nyatoh, in shaping the downstream flow patterns that fostered these significant outbreaks. The retraction of the North Pacific jet stream (NPJ) and subsequent excitation of Rossby wave packets played a critical role in establishing the amplified meridional flow pattern over the CONUS, providing a favorable environment for severe weather. This evolution was further enhanced by the anomalously warm Gulf of America/Gulf of Mexico sea surface temperatures, which contributed to a higher-than-usual convective instability in the surface warm sector.

This work underscores the need to better understand the physical mechanisms that link upstream processes, such as recurving tropical cyclones and NPJ retractions, to downstream severe weather outbreaks. Recognition of these upstream influences in the medium to extended forecast range may provide valuable opportunities to enhance predictability, especially during the cool season when severe convective weather is less frequent but often more impactful. Future research should continue to explore the coupling between tropical and extratropical processes, particularly how they modify the jet

stream and influence synoptic regimes favorable (or unfavorable) for severe convective weather.

Acknowledgments. The authors thank Drs. Andrew Winters, Harold Brooks, John Allen, Patrick Marsh, Mike Baldwin, and Adam Clark for discussions that benefited this manuscript. K. A. H. was provided support for this work by NOAA/Office of Oceanic and Atmospheric Research under NOAA-University of Oklahoma Cooperative Agreement NA21OAR4320204, U.S. Department of Commerce. Additional funding support for K. A. H. was provided by the NSF Climate and Large-Scale Dynamics program Awards 2039388 and the NOAA Research Global-Nest Initiative. V. A. G. was supported by National Science Foundation Award 2048770. This work comprised regular duties at the federally funded NOAA/NSSL for T. J. G.

Data availability statement. The GEFS analysis data used in this study are available in a publicly accessible repository hosted by Amazon Web Services at https://registry.opendata.aws/noaa-gefs, respectively. The GEFS reanalysis data were obtained from ftp://ftp.emc.ncep.noaa.gov/GEFSv12/reanalysis/FV3_reanalysis/. NCEP-NCAR reanalysis data were obtained from NOAA Physical Sciences Laboratory at https://psl.noaa.gov/data/gridded/data.ncep.reanalysis.html. Severe weather report data from the Storm Prediction Center are available online at https://www.spc.noaa.gov/wcm/#data. GridSat data were obtained from https://www.ncei.noaa.gov/thredds/catalog/cdr/gridsat/catalog.html, and daily maximum temperature records are freely available and retrieved from NOAA/NCEI online daily weather records at https://www.ncdc.noaa.gov/cdo-web/datatools/records. North Pacific jet phase data were obtained from (Winters 2021a) and are available at https://scholar.colorado.edu/concern/datasets/h702q753c. SFCOA data were available internally by SPC on NSSL computing systems. SST data are freely available online at https://coralreefwatch.noaa.gov/product/5km/. Codes used to generate the results herein are available from the authors upon request.

APPENDIX

Formula for Significant Tornado Parameter

The effective-layer formulation of the significant tornado parameter (Thompson et al. 2012) is defined as

$$\mathrm{STP} = \underbrace{\left(\frac{\mathrm{MLCAPE}}{1500\ \mathrm{J\ kg^{-1}}}\right)}_{a} \times \underbrace{\left(\frac{2000 - \mathrm{MLLCL}}{1000\ \mathrm{m}}\right)}_{b} \times \underbrace{\left(\frac{\mathrm{ESRH}}{150\ \mathrm{m^2\ s^{-2}}}\right)}_{c} \times \underbrace{\left(\frac{\mathrm{EBWD}}{20\ \mathrm{m\ s^{-1}}}\right)}_{d} \times \underbrace{\left(\frac{200 + \mathrm{MLCCIN}}{150\ \mathrm{J\ kg^{-1}}}\right)}_{e}$$

where MLCAPE is 100-hPa mixed-layer CAPE, MLCIN is 100-hPa mixed-layer CIN, MLLCL is 100-hPa mixed-layer lifted condensation level, ESRH is effective-layer storm-relative helicity, and EBWD is effective-layer bulk wind difference. The following terms are set to specific values given the following imposed conditions:

1) Term b $\begin{cases} 0 : \mathrm{MLLCL} > 2000\ \mathrm{m} \\ 1 : \mathrm{MLLCL} < 1000\ \mathrm{m} \end{cases}$

2) Term d $\begin{cases} 0 : \mathrm{EBWD} < 12.5\ \mathrm{m\ s^{-1}} \\ 1.5 : \mathrm{EBWD} > 30\ \mathrm{m\ s^{-1}} \end{cases}$

3) Term e $\begin{cases} 0 : \mathrm{MLCIN} < -200\ \mathrm{J\ kg^{-1}} \\ 1 : \mathrm{MLCIN} > -50\ \mathrm{J\ kg^{-1}} \end{cases}$

The STP index itself is set to zero when the base of the effective inflow layer is above the ground.

REFERENCES

Aiyyer, A., 2015: Recurving western North Pacific tropical cyclones and midlatitude predictability. *Geophys. Res. Lett.*, **42**, 7799–7807, https://doi.org/10.1002/2015GL065082.

Anwender, D., P. A. Harr, and S. C. Jones, 2008: Predictability associated with the downstream impacts of the extratropical transition of tropical cyclones: Case studies. *Mon. Wea. Rev.*, **136**, 3226–3247, https://doi.org/10.1175/2008MWR2249.1.

Archambault, H. M., L. F. Bosart, D. Keyser, and J. M. Cordeira, 2013: A climatological analysis of the extratropical flow response to recurving western North Pacific tropical cyclones. *Mon. Wea. Rev.*, **141**, 2325–2346, https://doi.org/10.1175/MWR-D-12-00257.1.

——, D. Keyser, L. F. Bosart, C. A. Davis, and J. M. Cordeira, 2015: A composite perspective of the extratropical flow response to recurving western North Pacific tropical cyclones. *Mon. Wea. Rev.*, **143**, 1122–1141, https://doi.org/10.1175/MWR-D-14-00270.1.

Ashley, W. S., A. J. Krmenec, and R. Schwantes, 2008: Vulnerability due to nocturnal tornadoes. *Wea. Forecasting*, **23**, 795–807, https://doi.org/10.1175/2008WAF2222132.1.

Bosart, L. F., B. J. Moore, J. M. Cordeira, and H. M. Archambault, 2017: Interactions of North Pacific tropical, midlatitude, and polar disturbances resulting in linked extreme weather events over North America in October 2007. *Mon. Wea. Rev.*, **145**, 1245–1273, https://doi.org/10.1175/MWR-D-16-0230.1.

Burg, T, and S. P. Lillo, 2021: Tropycal: A Python package for analyzing tropical cyclones and more. *34th Conf. on Hurricanes and Tropical Meteorology*, Online, Amer. Meteor. Soc., 16B.9, https://ams.confex.com/ams/34HURR/meetingapp.cgi/Paper/373965.

Byun, K.-Y., and T.-Y. Lee, 2012: Remote effects of tropical cyclones on heavy rainfall over the Korean peninsula—statistical and composite analysis. *Tellus*, **64A**, 14983, https://doi.org/10.3402/tellusa.v64i0.14983.

Childs, S. J., R. S. Schumacher, and J. T. Allen, 2018: Cold-season tornadoes: Climatological and meteorological insights. *Wea. Forecasting*, **33**, 671–691, https://doi.org/10.1175/WAF-D-17-0120.1.

Coniglio, M. C., and R. E. Jewell, 2022: SPC mesoscale analysis compared to field-project soundings: Implications for supercell environment studies. *Mon. Wea. Rev.*, **150**, 567–588, https://doi.org/10.1175/MWR-D-21-0222.1.

Cordeira, J. M., and L. F. Bosart, 2010: The antecedent large-scale conditions of the "Perfect Storms" of late October and early

November 1991. *Mon. Wea. Rev.*, **138**, 2546–2569, https://doi.org/10.1175/2010MWR3280.1.

Crisp, C. A., and J. M. Lewis, 1992: Return flow in the Gulf of Mexico. Part I: A classificatory approach with a global historical perspective. *J. Appl. Meteor.*, **31**, 868–881, https://doi.org/10.1175/1520-0450(1992)031<0868:RFITGO>2.0.CO;2.

Davis, C., C. Snyder, and A. C. Didlake Jr., 2008: A vortex-based perspective of eastern Pacific tropical cyclone formation. *Mon. Wea. Rev.*, **136**, 2461–2477, https://doi.org/10.1175/2007MWR2317.1.

Dawson, A., 2016: Windspharm: A high-level library for global wind field computations using spherical harmonics. *J. Open Res. Software*, **4**, e31, https://doi.org/10.5334/jors.129.

Durre, I., A. Arguez, C. J. Schreck III, M. F. Squires, and R. S. Vose, 2022: Daily high-resolution temperature and precipitation fields for the contiguous United States from 1951 to present. *J. Atmos. Oceanic Technol.*, **39**, 1837–1855, https://doi.org/10.1175/JTECH-D-22-0024.1.

Gahtan, J., K. R. Knapp, C. J. Schreck III, H. J. Diamond, J. P. Kossin, and M. C. Kruk, 2024: International Best Track Archive for Climate Stewardship (IBTrACS) Project, version 4.01. NOAA National Centers for Environmental Information, accessed 3 September 2024, https://doi.org/10.25921/82ty-9e16.

Galarneau, T. J., Jr., 2015: Influence of a predecessor rain event on the track of Tropical Cyclone Isaac (2012). *Mon. Wea. Rev.*, **143**, 3354–3376, https://doi.org/10.1175/MWR-D-15-0053.1.

——, L. F. Bosart, and R. S. Schumacher, 2010: Predecessor rain events ahead of tropical cyclones. *Mon. Wea. Rev.*, **138**, 3272–3297, https://doi.org/10.1175/2010MWR3243.1.

Gaza, R. S., and L. F. Bosart, 1990: Trough-merger characteristics over North America. *Wea. Forecasting*, **5**, 314–331, https://doi.org/10.1175/1520-0434(1990)005<0314:TMCONA>2.0.CO;2.

Gensini, V. A., D. Gold, J. T. Allen, and B. S. Barrett, 2019: Extended U.S. Tornado outbreak during late May 2019: A forecast of opportunity. *Geophys. Res. Lett.*, **46**, 10 150–10 158, https://doi.org/10.1029/2019GL084470.

——, A. M. Haberlie, and P. T. Marsh, 2020: Practically perfect hindcasts of severe convective storms. *Bull. Amer. Meteor. Soc.*, **101**, E1259–E1278, https://doi.org/10.1175/BAMS-D-19-0321.1.

Grams, C. M., and H. M. Archambault, 2016: The key role of diabatic outflow in amplifying the midlatitude flow: A representative case study of weather systems surrounding western North Pacific extratropical transition. *Mon. Wea. Rev.*, **144**, 3847–3869, https://doi.org/10.1175/MWR-D-15-0419.1.

——, S. C. Jones, C. A. Davis, P. A. Harr, and M. Weissmann, 2013a: The impact of Typhoon Jangmi (2008) on the midlatitude flow. Part I: Upper-level ridgebuilding and modification of the jet. *Quart. J. Roy. Meteor. Soc.*, **139**, 2148–2164, https://doi.org/10.1002/qj.2091.

——, ——, and ——, 2013b: The impact of Typhoon Jangmi (2008) on the midlatitude flow. Part II: Downstream evolution. *Quart. J. Roy. Meteor. Soc.*, **139**, 2165–2180, https://doi.org/10.1002/qj.2119.

——, S. T. K. Lang, and J. H. Keller, 2015: A quantitative assessment of the sensitivity of the downstream midlatitude flow response to extratropical transition of tropical cyclones. *Geophys. Res. Lett.*, **42**, 9521–9529, https://doi.org/10.1002/2015GL065764.

Griffin, K. S., and J. E. Martin, 2017: Synoptic features associated with temporally coherent modes of variability of the North Pacific jet stream. *J. Climate*, **30**, 39–54, https://doi.org/10.1175/JCLI-D-15-0833.1.

Guan, H., and Coauthors, 2022: GEFSv12 reforecast dataset for supporting subseasonal and hydrometeorological applications. *Mon. Wea. Rev.*, **150**, 647–665, https://doi.org/10.1175/MWR-D-21-0245.1.

Guastini, C. T., and L. F. Bosart, 2016: Analysis of a progressive derecho climatology and associated formation environments. *Mon. Wea. Rev.*, **144**, 1363–1382, https://doi.org/10.1175/MWR-D-15-0256.1.

Guyer, J., 2022: The 2021 Tornado season: December devastation. *Weatherwise*, **75**, 34–41, https://doi.org/10.1080/00431672.2022.2065861.

Hamill, T. M., and Coauthors, 2022: The reanalysis for the Global Ensemble Forecast System, version 12. *Mon. Wea. Rev.*, **150**, 59–79, https://doi.org/10.1175/MWR-D-21-0023.1.

Heming, J. T., and Coauthors, 2019: Review of recent progress in tropical cyclone track forecasting and expression of uncertainties. *Trop. Cyclone Res. Rev.*, **8**, 181–218, https://doi.org/10.1016/j.tcrr.2020.01.001.

Hitchens, N. M., H. E. Brooks, and M. P. Kay, 2013: Objective limits on forecasting skill of rare events. *Wea. Forecasting*, **28**, 525–534, https://doi.org/10.1175/WAF-D-12-00113.1.

Hsu, S., 1997: Effects of cold air outbreaks on evaporation and heat loss from three regions in the Gulf of Mexico. *Gulf Mex. Sci.*, **15**, 2, https://doi.org/10.18785/goms.1502.02.

Jaffe, S. C., J. E. Martin, D. J. Vimont, and D. J. Lorenz, 2011: A synoptic climatology of episodic, subseasonal retractions of the Pacific jet. *J. Climate*, **24**, 2846–2860, https://doi.org/10.1175/2010JCLI3995.1.

Jiang, N., B. Liu, C. Zhu, and Y. Chen, 2023: Remote linkage of record-breaking U.S. Tornado outbreaks to the tropical cyclone in western North Pacific in December 2021. *Environ. Res. Lett.*, **18**, 044036, https://doi.org/10.1088/1748-9326/acc880.

Johns, R. H., and W. D. Hirt, 1987: Derechos: Widespread convectively induced windstorms. *Wea. Forecasting*, **2**, 32–49, https://doi.org/10.1175/1520-0434(1987)002<0032:DWCIW>2.0.CO;2.

Kalnay, E., and Coauthors, 1996: The NCEP/NCAR 40-Year Reanalysis Project. *Bull. Amer. Meteor. Soc.*, **77**, 437–471, https://doi.org/10.1175/1520-0477(1996)077<0437:TNYRP>2.0.CO;2.

Keller, J. H., and Coauthors, 2019: The extratropical transition of tropical cyclones. Part II: Interaction with the midlatitude flow, downstream impacts, and implications for predictability. *Mon. Wea. Rev.*, **147**, 1077–1106, https://doi.org/10.1175/MWR-D-17-0329.1.

Kim, D., S.-K. Lee, H. Lopez, J.-H. Jeong, and J.-S. Hong, 2024: An unusually prolonged Pacific-North American pattern promoted the 2021 winter quad-state tornado outbreaks. *npj Climate Atmos. Sci.*, **7**, 133, https://doi.org/10.1038/s41612-024-00688-0.

Knapp, K. R., M. C. Kruk, D. H. Levinson, H. J. Diamond, and C. J. Neumann, 2010: The International Best Track Archive for Climate Stewardship (IBTrACS). *Bull. Amer. Meteor. Soc.*, **91**, 363–376, https://doi.org/10.1175/2009BAMS2755.1.

——, and Coauthors, 2011: Globally gridded satellite observations for climate studies. *Bull. Amer. Meteor. Soc.*, **92**, 893–907, https://doi.org/10.1175/2011BAMS3039.1.

Leicht, T. C., and L. F. Bosart, 2024: Assessment of the dynamical linkages and flow evolution governing multiple extreme

weather events over western North America in February 2019. *Mon. Wea. Rev.*, **152**, 2055–2073, https://doi.org/10.1175/MWR-D-24-0040.1.

Lewis, J. M., C. M. Hayden, R. T. Merrill, and J. M. Schneider, 1989: Gufmex: A study of return flow in the Gulf of Mexico. *Bull. Amer. Meteor. Soc.*, **70**, 24–29, https://doi.org/10.1175/1520-0477(1989)070<0024:GASORF>2.0.CO;2.

Madsen, M. M., and J. E. Martin, 2023: A self-organizing maps analysis of wintertime North Pacific jet stream variability. *J. Climate*, **36**, 1863–1879, https://doi.org/10.1175/JCLI-D-22-0452.1.

Maruf, R., and Reuters, 2021: Amazon warehouse collapses after tornado leaves at least two dead. *CNN Business*, 11 December, https://www.cnn.com/2021/12/11/business/amazon-warehouse-edwardsville-tornado/index.html.

Maturi, E., A. Harris, J. Mittaz, J. Sapper, G. Wick, X. Zhu, P. Dash, and P. Koner, 2017: A new high-resolution sea surface temperature blended analysis. *Bull. Amer. Meteor. Soc.*, **98**, 1015–1026, https://doi.org/10.1175/BAMS-D-15-00002.1.

McTaggart-Cowan, R., J. R. Gyakum, and M. K. Yau, 2001: Sensitivity testing of extratropical transitions using potential vorticity inversions to modify initial conditions: Hurricane earl case study. *Mon. Wea. Rev.*, **129**, 1617–1636, https://doi.org/10.1175/1520-0493(2001)129<1617:STOETU>2.0.CO;2.

——, ——, and ——, 2004: The impact of tropical remnants on extratropical cyclogenesis: Case study of Hurricanes Danielle and Earl (1998). *Mon. Wea. Rev.*, **132**, 1933–1951, https://doi.org/10.1175/1520-0493(2004)132<1933:TIOTRO>2.0.CO;2.

Miller, D. E., and V. A. Gensini, 2023: GEFSv12 high- and low-skill day-10 tornado forecasts. *Wea. Forecasting*, **38**, 1195–1207, https://doi.org/10.1175/WAF-D-22-0122.1.

——, ——, and B. S. Barrett, 2022: Madden-Julian oscillation influences United States springtime tornado and hail frequency. *npj Climate Atmos. Sci.*, **5**, 37, https://doi.org/10.1038/s41612-022-00263-5.

Molina, M. J., and J. T. Allen, 2019: On the moisture origins of tornadic thunderstorms. *J. Climate*, **32**, 4321–4346, https://doi.org/10.1175/JCLI-D-18-0784.1.

——, and ——, 2020: Regionally-stratified tornadoes: Moisture source physical reasoning and climate trends. *Wea. Climate Extremes*, **28**, 100244, https://doi.org/10.1016/j.wace.2020.100244.

——, R. P. Timmer, and J. T. Allen, 2016: Importance of the Gulf of Mexico as a climate driver for U.S. severe thunderstorm activity. *Geophys. Res. Lett.*, **43**, 12 295–12 304, https://doi.org/10.1002/2016GL071603.

——, J. T. Allen, and V. A. Gensini, 2018: The Gulf of Mexico and ENSO influence on subseasonal and seasonal CONUS winter tornado variability. *J. Appl. Meteor. Climatol.*, **57**, 2439–2463, https://doi.org/10.1175/JAMC-D-18-0046.1.

——, ——, and A. F. Prein, 2020: Moisture attribution and sensitivity analysis of a winter tornado outbreak. *Wea. Forecasting*, **35**, 1263–1288, https://doi.org/10.1175/WAF-D-19-0240.1.

Moore, B. J., L. F. Bosart, D. Keyser, and M. L. Jurewicz, 2013: Synoptic-scale environments of predecessor rain events occurring east of the Rocky Mountains in association with Atlantic basin tropical cyclones. *Mon. Wea. Rev.*, **141**, 1022–1047, https://doi.org/10.1175/MWR-D-12-00178.1.

NOAA, 2023: NOAA unified surface analysis fronts. Zenodo, accessed 9 May 2023, https://doi.org/10.5281/zenodo.7505022.

Quinting, J. F., and S. C. Jones, 2016: On the impact of tropical cyclones on Rossby wave packets: A climatological perspective. *Mon. Wea. Rev.*, **144**, 2021–2048, https://doi.org/10.1175/MWR-D-14-00298.1.

Riboldi, J., C. M. Grams, M. Riemer, and H. M. Archambault, 2019: A phase locking perspective on Rossby wave amplification and atmospheric blocking downstream of recurving western North Pacific tropical cyclones. *Mon. Wea. Rev.*, **147**, 567–589, https://doi.org/10.1175/MWR-D-18-0271.1.

Rolph, G., A. Stein, and B. Stunder, 2017: Real-time Environmental Applications and Display sYstem: READY. *Environ. Modell. Software*, **95**, 210–228, https://doi.org/10.1016/j.envsoft.2017.06.025.

Sherburn, K. D., and M. D. Parker, 2014: Climatology and ingredients of significant severe convection in high-shear, low-CAPE environments. *Wea. Forecasting*, **29**, 854–877, https://doi.org/10.1175/WAF-D-13-00041.1.

——, ——, J. R. King, and G. M. Lackmann, 2016: Composite environments of severe and nonsevere high-shear, low-CAPE convective events. *Wea. Forecasting*, **31**, 1899–1927, https://doi.org/10.1175/WAF-D-16-0086.1.

Sodemann, H., C. Schwierz, and H. Wernli, 2008: Interannual variability of Greenland winter precipitation sources: Lagrangian moisture diagnostic and North Atlantic oscillation influence. *J. Geophys. Res.*, **113**, D03107, https://doi.org/10.1029/2007JD008503.

SPC, 2024: Storm Prediction Center severe weather database. Accessed 3 September 2024, https://www.spc.noaa.gov/wcm.

Squitieri, B. J., A. R. Wade, and I. L. Jirak, 2023: A historical overview on the science of derechos: Part I: Identification, climatology, and societal impacts. *Bull. Amer. Meteor. Soc.*, **104**, E1709–E1733, https://doi.org/10.1175/BAMS-D-22-0217.1.

Stein, A. F., R. R. Draxler, G. D. Rolph, B. J. B. Stunder, M. D. Cohen, and F. Ngan, 2015: NOAA'S HYSPLIT atmospheric transport and dispersion modeling system. *Bull. Amer. Meteor. Soc.*, **96**, 2059–2077, https://doi.org/10.1175/BAMS-D-14-00110.1.

Strader, S. M., W. S. Ashley, A. M. Haberlie, and K. Kaminski, 2022: Revisiting U.S. nocturnal tornado vulnerability and its influence on tornado impacts. *Wea. Climate Soc.*, **14**, 1147–1163, https://doi.org/10.1175/WCAS-D-22-0020.1.

Thompson, R. L., 2023: A comparison of right-moving supercell and quasi-linear convective system tornadoes in the contiguous United States 2003–21. *Wea. Forecasting*, **38**, 1497–1513, https://doi.org/10.1175/WAF-D-23-0006.1.

——, B. T. Smith, J. S. Grams, A. R. Dean, and C. Broyles, 2012: Convective modes for significant severe thunderstorms in the contiguous United States. Part II: Supercell and QLCS tornado environments. *Wea. Forecasting*, **27**, 1136–1154, https://doi.org/10.1175/WAF-D-11-00116.1.

Van Den Broeke, M. S., M. B. Wilson, C. A. Van Den Broeke, D. J. Healey, M. J. Wood, and R. E. Nelson, 2023: Polarimetric radar observations of a long-lived supercell and associated tornadoes on 10–11 December 2021. *Mon. Wea. Rev.*, **151**, 2501–2520, https://doi.org/10.1175/MWR-D-22-0330.1.

Villanueva, E. E., V. M. Mendoza, and J. Adem, 2010: Sea surface temperature and mixed layer depth changes due to cold-air outbreak in the Gulf of Mexico. *Atmósfera*, **23**, 325–346.

Wade, A. R., and M. D. Parker, 2021: Dynamics of simulated high-shear, low-CAPE supercells. *J. Atmos. Sci.*, **78**, 1389–1410, https://doi.org/10.1175/JAS-D-20-0117.1.

Wallace, J. M., and D. S. Gutzler, 1981: Teleconnections in the geopotential height field during the Northern Hemisphere winter. *Mon. Wea. Rev.*, **109**, 784–812, https://doi.org/10.1175/1520-0493(1981)109<0784:TITGHF>2.0.CO;2.

Wang, J., and Coauthors, 2023: Soil moisture observations from shortwave infrared channels reveal tornado tracks: A case in 10–11 December 2021 tornado outbreak. *Geophys. Res. Lett.*, **50**, e2023GL102984, https://doi.org/10.1029/2023GL102984.

Warner, M. S. C., 2018: Introduction to PySPLIT: A python toolkit for NOAA ARL'S HYSPLIT model. *Comput. Sci. Eng.*, **20**, 47–62, https://doi.org/10.1109/MCSE.2017.3301549.

Weiss, S. J., 1992: Some aspects of forecasting severe thunderstorms during cool-season return-flow episodes. *J. Appl. Meteor.*, **31**, 964–982, https://doi.org/10.1175/1520-0450(1992)031<0964:SAOFST>2.0.CO;2.

Winters, A. C., 2021a: The state of the North Pacific jet and North Atlantic jet in the context of their two leading modes of variability. University of Colorado Boulder, accessed 5 February 2024, https://doi.org/10.25810/CKN0-GP39.

——, 2021b: Subseasonal prediction of the state and evolution of the North Pacific jet stream. *J. Geophys. Res. Atmos.*, **126**, e2021JD035094, https://doi.org/10.1029/2021JD035094.

——, and H. E. Attard, 2022: North Pacific and North Atlantic jet covariability and its relationship to cool season temperature and precipitation extremes. *Wea. Forecasting*, **37**, 1581–1600, https://doi.org/10.1175/WAF-D-21-0203.1.

——, L. F. Bosart, and D. Keyser, 2019a: Antecedent North Pacific jet regimes conducive to the development of continental U.S. extreme temperature events during the cool season. *Wea. Forecasting*, **34**, 393–414, https://doi.org/10.1175/WAF-D-18-0168.1.

——, D. Keyser, and L. F. Bosart, 2019b: The development of the North Pacific jet phase diagram as an objective tool to monitor the state and forecast skill of the upper-tropospheric flow pattern. *Wea. Forecasting*, **34**, 199–219, https://doi.org/10.1175/WAF-D-18-0106.1.

Zavala-Hidalgo, J., R. Romero-Centeno, A. Mateos-Jasso, S. L. Morey, and B. Martínez-López, 2014: The response of the Gulf of Mexico to wind and heat flux forcing: What has been learned in recent years? *Atmósfera*, **27**, 317–334, https://doi.org/10.1016/S0187-6236(14)71119-1.

Zimin, A. V., I. Szunyogh, B. R. Hunt, and E. Ott, 2006: Extracting envelopes of nonzonally propagating Rossby wave packets. *Mon. Wea. Rev.*, **134**, 1329–1333, https://doi.org/10.1175/MWR3122.1.